Investigating the response of Greenland and Antarctic glaciers to atmospheric and oceanic forcings using a 1D flowline model

By

Konstantinos Petrakopoulos

Submitted to the Department of Geology and the
Graduate Faculty of the University of Kansas
in partial fulfillment of the requirements for the degree of
Doctor of Philosophy

Leigh A. Stearns, Chair

C.J. van der Veen, Co-chair

George Tsoflias

Andrea E. Brookfield

Dave Z. Besson

Date defended: May 09, 2017

The Thesis Committee for Konstantinos Petrakopoulos certifies
that this is the approved version of the following thesis :

Investigating the response of Greenland and Antarctic glaciers to atmospheric and oceanic forcings using a 1D flowline model

Leigh A. Stearns, Chair

Date approved: July 26, 2017

Abstract

Over the past two decades, the mass loss from the Antarctic and Greenland ice sheets has contributed approximately 11.2 ± 3.8 mm to global mean sea level, one third of the total sea level rise since the 1990s. The majority of this mass loss has come from the acceleration of tidewater outlet glaciers, through mechanisms that are poorly understood. While we know that the recent increase in mass loss is due to climate changes, questions remain about the processes that both destabilize and stabilize glaciers. Being able to characterize these processes is essential for producing realistic ice sheet mass balance predictions. In this dissertation, we use a width average (1-D) flowline model to investigate the current and past behavior of glaciers in both Antarctica and Greenland, with the broader goal of understanding how they respond to increased climate variability. In the first chapter, we show that the unique behavior of Helheim Glacier in East Greenland is driven primarily by atmospheric, not ocean variability. In the second chapter, we address the role of glacier geometry in modulating decadal-scale dynamics of Greenland glaciers. Our results show that, contrary to many assumptions, width and bed topography only play a small role in controlling mass loss during retreat. The third chapter focuses on the retreat of Byrd Glacier, East Antarctica from its grounding line during the Last Glacial Maximum (LGM), to its current configuration, under rising atmospheric and oceanic temperatures. We show that atmospheric changes are the primary driver for the retreat, and that the current geometry of the Ross Ice Shelf has been similar for the last 2,000 years. The results of this thesis increase our knowledge of Greenland and Antarctic glacier dynamics, their relationship with atmospheric and oceanic forcings, and their future contribution to sea-level.

Acknowledgements

Andy Aschwanden, Aristeidis Papagiannopoulos, Brice Noël, Christian Schoof, Ellyn Enderlin, Epperson, Riley James, Faezeh Nick, Isabella Stavroula Frangouli, José Vélez González, Logan Byers, Rhonda Houser, Sarah F. Child, Steve Foga, Sue Cook, Tracy Hirata-Edds, Xuemin Tu.

Contents

List of Figures

INTRODUCTION

The largest potential reservoirs of sea level rise are the Greenland and Antarctic ice sheets. Combined, the ice sheets contain 69% of the Earth's fresh water (Gleick, 1993), and their total collapse would raise eustatic sea level by 63.9 m (Bindoff et al., 2007). More than 10% of the world's population lives close to the coastline, and even a modest rise in sea level would have disastrous physical and economic consequences (McGranahan et al., 2007). An intermediate climate scenario predicts 1 m of sea level rise by 2100, followed by an unstoppable increase (Levermann et al., 2013; Kopp et al., 2014).

This dissertation is geared towards understanding why and how tidewater outlet glaciers in Greenland and Antarctica respond to changes in climate. While many different observational platforms show stark patterns of glacier retreat, thinning and acceleration, very little is known about the physical processes controlling this behavior. We present a new one-dimensional flowline model that allows us to investigate glacier response to a variety of different perturbations and geometries. By constraining this model with observational data, we address some important and fundamental questions in glaciology, including: Does the ocean or atmosphere drive current ice mass loss in Greenland (chapter 1)? How important is bed geometry in modulating glacier response to climate changes (chapter 2)? Are oceanic or atmospheric perturbations responsible for Antarctic mass loss since the LGM (chapter 3)?

Chapter 1: Investigating the response of Helheim Glacier to perturbations using a one dimensional flowline model

1.0 INTRODUCTION

Over the last two decades, the mass loss of the Greenland Ice Sheet (GrIS) has nearly doubled (Shepherd et al., 2012; McMillan et al., 2016), with nearly half of this mass loss attributed to the acceleration of outlet glaciers and the remainder due to enhanced surface melt (e.g. Rignot et al., 2008; van den Broeke et al., 2009; Sasgen et al., 2012). Despite numerous observations of GrIS marine-terminating glacier acceleration (e.g.Rignot et al., 2011b; Moon et al., 2012; Csatho et al., 2014), thinning (Krabill et al., 2004; Luckman et al., 2006; Stearns et al., 2008; Pritchard et al., 2009) and retreat (Howat et al., 2008; Moon & Joughin, 2008), questions remain about the processes that link sudden changes in outlet glaciers to climate.

The mechanisms driving marine outlet glacier variability are poorly understood yet critical to improving projections of ice sheet mass balance. In particular, the processes that control glacier acceleration are disputed, with the central issue being whether flow accelerations initiate at the terminus or along the glacier trunk. Several studies using observational data and numerical models of Greenland outlet glaciers suggest that enhanced calving triggers a dynamic change in flow speed, which rapidly propagates up-glacier (e.g. Nick et al., 2009; Pritchard et al., 2009; Nick et al., 2010). Other studies suggest that acceleration is initiated by changes in ice rheology and subglacier water availability, and that increased calving is simply a consequence of upflow acceleration (e.g. van der Veen et al., 2011; Bevan et al., 2015). The near-coincident timing of acceleration, thinning and retreat, and the complex relationship between ice dynamics and environmental forcings inhibits our understanding of glacier variability. Numerical models are necessary to investigate the sensitivity and response of tidewater glaciers to perturbations at different boundaries, in particular at the bed and terminus.

Between 2002 and 2005 the terminus of Helheim Glacier accelerated from 8 km yr^{-1} to 11 km yr^{-1} , thinned by over 100 m, and retreated 5 km (Howat et al., 2005; Luckman et al., 2006; Stearns & Hamilton, 2007). While Helheim Glacier did decelerate, thicken and advance beginning in 2006, it did not return to its pre-2002 geometry (Howat et al., 2007; Bevan et al., 2012). Acceleration

and thinning extended up to 80 km up-glacier, reaching a maximum rate between 2004 and 2005 (Howat et al., 2007; Bevan et al., 2012). Between 2001 and 2016, Helheim Glacier retreated 5 km, but radar echograms (Leuschen & Allen, 2011) show that Helheim Glacier's grounding line position did not change substantially. In this study we use a standard flowline model to investigate the unique pattern of rapid acceleration and retreat, followed by deceleration and advance.

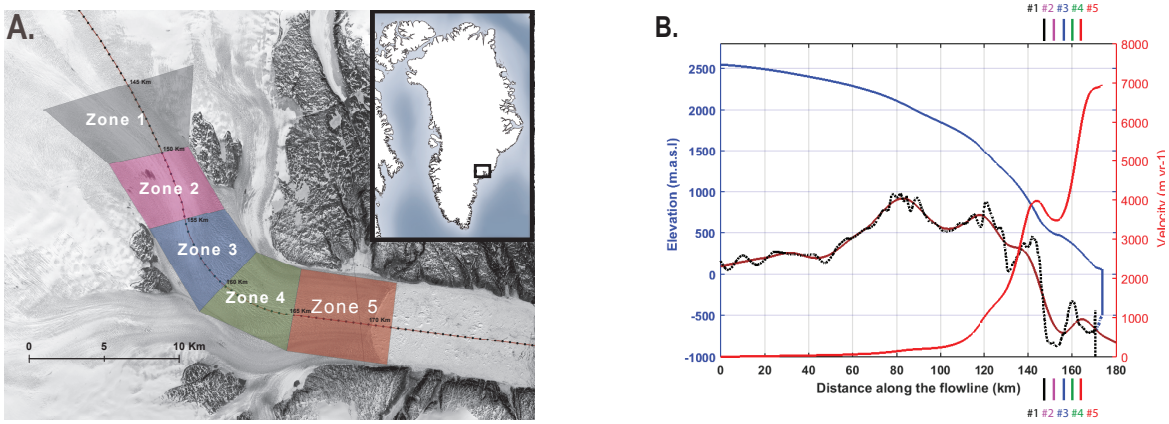

Figure 1: A) Delineation of the five zones used in this study, each roughly 5 km long, extending from the equilibrium line altitude (ELA) to the terminus of Helheim Glacier, East Greenland. B). Smoothed geometry and ice velocity of Helheim Glacier in steady state. The dashed black line shows the mass conserving bed topography for Helheim Glacier (Morlighem et al., 2014) along the flowline in panel A. The 5 vertical lines represent the up-flow extent of the zones shown in panel A.

2.0 METHODS

To examine the sensitivity of Helheim Glacier to perturbations at the bed and terminus, we use a one-dimensional, width-averaged, depth-integrated, full stress, flow-band model, based on the assumption of planar flow (similar to Vieli & Payne, 2005; Nick et al., 2010; Vieli & Nick, 2011). We are interested in how perturbations, both at the terminus and along the glacier trunk, can impact ice discharge across the grounding line. In particular, we adjust variables at the terminus (calving rate, submarine melt rate, and mélange rigidity) and along the glacier trunk (basal sliding) to assess how the glacier responds to individual, and a combination of, forcings. To characterize the along-flow response to changes in basal sliding, we divide the region between the equilibrium line

altitude (ELA) and the terminus into five zones (Figure 1A), and adjust basal sliding in each zone. All model experiments start from a steady state condition and run for 15 years (Figure 1B).

2.1 Numerical Model

Glacier flow is described mathematically through the force balance equation, where the gravitational driving stress is balanced by three resistive stresses: basal drag, lateral drag, and gradients in longitudinal stress (Whillans & van Der Veen, 1997; van der Veen, 2013). Our flowline model, which is consistent with the mathematical approach used by Nick et al. (2010), adopts the modified Weertman sliding relation where basal drag is related to effective pressure and proportional to the width-averaged sliding velocity (van der Veen, 1996). This sliding relation assumes an easy connection between the subglacial drainage system and the open ocean, such that the effective pressure, P_{eff}, at the terminus is equal to the height above buoyancy, H_{buoy} (van der Veen, 2013). For numerical stability, we use a small time step (0.0027 years) to satisfy the Courant - Friedrichs - Lewy (CFL) condition (Morton & Mayers, 2005). With the exponent of Glen's flow law, n, equal to 3, we solve the following equation:

$$-(AS)\,[(H-\frac{\rho_w}{\rho_i}\,|H_{base}|)\,U]^{\frac{1}{3}}-2\frac{H}{W_{full}}\,(\frac{5U}{AW_{full}})^{\frac{1}{3}}+2\{\frac{\partial}{\partial x}[HA^{-\frac{1}{3}}|\frac{\partial U}{\partial x}|^{-\frac{2}{3}}\frac{\partial U}{\partial x}]\}=\rho_i\,g\,H\,(\frac{\partial H_s}{\partial x})\,, \tag{1}$$

where ρ_i is the ice density (917 kg m^{-3}), ρ_w is the ocean water density (1025 kg m^{-3}), and g is the gravitational acceleration (9.806 m s^{-2}). The distance along the flowline is x, H is the thickness of the glacier, H_{base} is the bed elevation (negative below sea level), W_{full} is the glacier width, H_s is the surface elevation, and U is the depth-integrated, width-averaged ice velocity. AS is the basal drag parameter which is fixed, and the exponent of the sliding relation, m, is set to 3. The rate factor A is set to 9.3 10^{-25} s^{-1} which is equivalent to a depth-average ice temperature of -5 °C (Cuffey & Paterson, 2010).

In the force balance equation (1), the terms on the left represent basal drag, lateral drag, and

longitudinal stress gradients, respectively; the term on the right is the gravitational driving stress. Equation (1) is a system of N non-linear ordinary differential equations (ODE) with two boundary conditions – at the ice divide and at the glacier terminus. N is the number of grid points in our flowline. We use the generalized Newton- Raphson method to calculate the ice velocity at each grid point using equation (1). For the first boundary condition, we set the horizontal velocity at the ice divide to zero. For the second boundary condition, we balance the difference between water pressure and ice overburden pressure with the horizontal stress at the terminus (Shumskiy & Krass, 1976). Following Nick et al. (2010), we allow the model to incorporate a small amount of backstress, σ_b, due to a persistent ice mélange at the calving front (Amundson & Truffer, 2010). The stretching rate at the calving front is defined as:

$$\left.\frac{\partial U(x)}{\partial x}\right|_{x=terminus} = A\,[\,\frac{\rho_i g}{4}(\,H(x) - \frac{H_{base}(x)^2}{H(x)} - 2\frac{\sigma_b}{\rho_i g}\,)\,]^3\,\Big|_{x=terminus}\,. \tag{2}$$

We extract the depth-integrated, width-averaged, glacier velocity (U) that satisfies equation (1) using the above boundary conditions and solve for the change in ice thickness (H) at each gridpoint, using the forward Euler method:

$$\frac{\partial H}{\partial t} = -\,(\,\frac{1}{W_{full}}\,)\,\frac{\partial(H\;U\;W_{full})}{\partial x} + S\dot{M}B\; + \dot{m}_{float}\;\;, \tag{3}$$

where $S\dot{M}B$ is the surface mass balance (SMB) rate, and $\dot{m}_{float}$ is the submarine melting rate, if a floating tongue exists. To determine if the glacier advances or retreats, we use the full crevasse calving criterion described by Benn et al. (2007). The model employs a moving-grid, which allows the terminus position to be tracked at each time step (Nick & Oerlemans, 2006). When the glacier changes length due to advance or retreat, a new grid is defined to fit the new length, with the last point at the terminus and the same number of grid points. This technique has the advantage of allowing the glacier to change length in increments that are smaller than the grid spacing. At each time step all the variables are interpolated onto the new grid (Nick et al., 2010).

Despite modifications in how we solve and parameterize our model, it is based on the same

equations and assumptions as Nick et al. (2009) and Nick et al. (2010). We validate our model by performing two experiments to assess our model's response to a basal sliding perturbation (similar to that found in Nick et al. (2009)) and a calving perturbation (similar to that found in Nick et al. (2010)).

The basal sliding perturbation experiments found in Nick et al. (2009), and that we do here, consist of a sudden increase in basal sliding along the final 15 km of the glacier that increases in magnitude closer to the terminus. In our model framework we progressively increase the sliding perturbation, from 10% in zone 3, to 35% in zone 4, and 70% in zone 5. After a 10 year perturbation, both models show thinning that extends 100 km up-flow, with a maximum amount of thinning in zone 3 (~25 km up-flow from the terminus). Both models also show a ~20% acceleration at terminus in year 1, which decreases to 5% by year 3. The terminus retreats less than 1 km, and the grounding line remains stationary in both models.

We use the calving criterion described in Nick et al (2010) and assess our model by repeating an experiment described in their study. Despite using different geometries and steady state profiles, our flowline experiments obtain similar results. With a 10% decrease in water level in surface crevasses, the glacier advances ~10 km. With a 40% increase in water level in surface crevasses, the glacier retreats ~7 km.

Based on the comparative results of these experiments, we show that our version of the flowline model is fundamentally similar to published models found in Nick et al. (2009), and Nick et al. (2010).

2.2 Calving Criterion

Our flowline model relates ice thickness at the terminus to glacier length through the calving criterion described by Benn et al. (2007). Our calving criterion produces stable glacier behavior when the glacier retreats into deeper water, and can simulate seasonal cycles of advance and retreat by incorporating seasonal water depth in crevasses (Nick et al., 2010). However, in order for calving to occur at the terminus of Helheim Glacier, where the ice is roughly 650 m thick (Sutherland &

Straneo, 2012), the calving criterion requires very large water depths (> 250 m). To resolve this issue, we modify the crevasse criterion so that calving can occur even in the absence of water-filled crevasses. Based on observations, we form surface crevasses near the ELA and have them grow as they advect down-flow. The depth of crevasses along the flowline (S) is the summation of penetration due to extensional local stresses at the terminus and crevasse depth from the growth and advection of crevasses that form up-flow.

The penetration of surface crevasses (Nick et al., 2010) is described as:

$$S(x) = \frac{(2(\frac{\frac{\partial U}{\partial x}}{A})^{\frac{1}{3}})}{\rho_i g} + \frac{\rho_{wf}}{\rho_i} D_{water} \quad , \tag{4}$$

and the extent of bottom crevasses along the flowline (Nick et al., 2010) is determined through:

$$B(x) = \frac{\rho_w}{\rho_w - \rho_i}(\frac{((\frac{\frac{\partial U}{\partial x}}{A})^{\frac{1}{3}})}{\rho_i g} - (H_{buoy}(x)) \quad . \tag{5}$$

The height-above-buoyancy, H_{buoy}, is defined by (van der Veen, 2013):

$$H_{buoy}(x) = H(x) + \frac{\rho_w}{\rho_i} H_{base}(x) \quad . \tag{6}$$

The original calving criterion assumes equal crevasse water depth in crevasses extending from the ELA to the terminus (Nick et al., 2010). We modify this distribution to more accurately represent crevasses by incorporating along-flow changes in crevasse size and water depth ($D_{water}(x)$). Using this modified criterion, we can set the distribution of crevasses and crevasse water depth to vary linearly or nonlinearly from the ELA to the terminus.

where ρ_{wf} is the density of fresh water (1028 kg m^{-3}), D_{water} is the height of water inside surface crevasses along the flowline, and S is the penetration depth of surface crevasses along the flowline (Benn et al., 2007). In our calving criterion, water inside surface crevasses increases the calving rate, but is not necessary for calving to occur because we allow crevasses to initiate far upflow and become progressively deeper with longitudinal stretching as they approach the terminus. By incorporating modifications that allow for the spatial variability in crevasse depth and amount of

water, we add flexibility and, what is likely a more realistic distribution of crevasses, to our model.

2.3 Perturbation types: Instantaneous and Variable

We assess glacier response to two very different types of perturbations: instantaneous perturbations and variable perturbations. Instantaneous perturbations simulate a rapid and step-wise perturbation to the boundary condition, which is useful in characterizing glacier response to individual perturbations. We also apply instantaneous perturbations for short time periods (3 and 6 months) to assess glacier response to short-lived (seasonal) perturbations.

With variable perturbations, parameters (e.g. sliding) are adjusted at each time step so that the model mimics the observed glacier behavior. In particular, the parameter is adjusted so that the model output falls within the 1% bounds of the observed discharge value or terminus position (Figure 2). This type of inverse model allows us to assess whether realistic boundary conditions can be used to model the observed glacier behavior.

2.4 Data input

Input data for our model includes bed topography (Morlighem et al., 2014), and surface topography (Howat et al., 2014), smoothed by a linear least squares regression and gridded to 250 m horizontal resolution. We use annual surface mass balance data in the ablation zone from the PROMICE database (Machguth et al., 2016) averaged from 2006-2010, and in the accumulation zone we use RACMO 2.3 data (Noël et al., 2015) at 1 km resolution. We apply a maximum submarine melt rate of -580 m yr^{-1} (Sutherland & Straneo, 2012), beginning one kilometer seaward of the terminus (Sciascia et al., 2013; Slater et al., 2017). The width-averaged terminus velocity data for Helheim Glacier is derived from a combination of optical (Howat, 2016) and radar satellite imagery (Joughin et al., 2010a; Joughin et al., 2010b). The changes in Helheim Glacier's terminus position are based on both optical and radar satellite imagery (Foga et al., 2014).

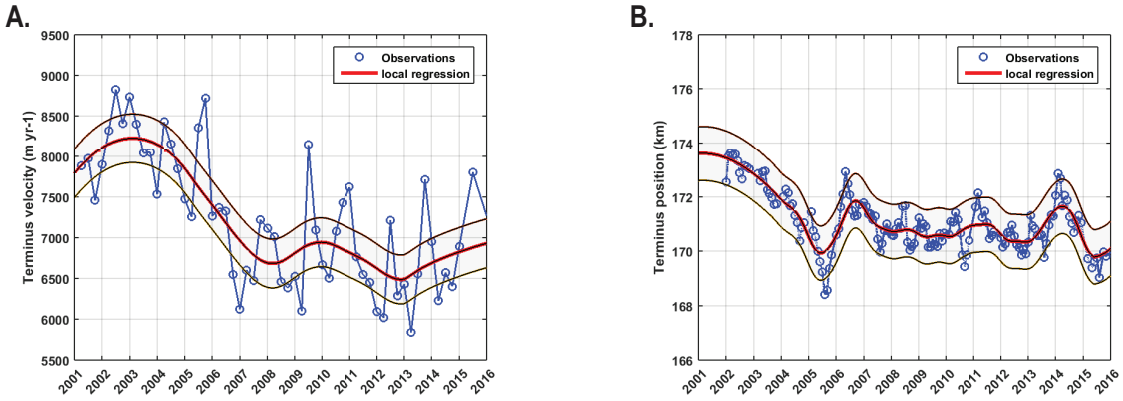

Figure 2: A) Width-averaged terminus velocity data for Helheim Glacier derived from a combination of optical (Howat, 2016) and radar satellite imagery (Joughin et al., 2010a; Joughin et al., 2010b). B) Width-averaged terminus positions for the same time period are also derived from optical and radar imagery (Foga et al., 2014). In both panels the red line is the local regression, and the grey shading represents the 1% bounds.

3.0 EXPERIMENTS

Our experiments are designed to investigate the mechanisms that caused the complex flow behavior of Helheim Glacier between 2001 and 2016. In particular, we assess whether variations in ice-bed or ice-ocean processes dictate flow variability. While some studies suggest that flow variability is predominantly driven by changes in water pressure at the ice-bed interface (e.g. van der Veen et al., 2011; Bevan et al., 2015), other studies suggest that they are initiated by changes at the ice-ocean interface (e.g. Nick et al., 2009; Murray et al., 2010; Rignot et al., 2010; Carr et al., 2015; Truffer & Motyka, 2016). The experiments described in this section assess how perturbations in basal sliding, iceberg calving, backstress pressure, and submarine melt impact the behavior of Helheim Glacier from 2001 - 2016. We conduct two types of experiments for each scenario: instantaneous perturbations and variable perturbations (described in Section 2.3).

3.1 Experiment #1: Increasing basal sliding

Basal sliding depends on many parameters including basal character (bed rigidity, permeability, and roughness) and subglacial hydrology (water pressure, types of subglacial channels, and amount

of water). In our flowline model, we use a sliding law for a hard-bedded glacier that is dependent on water availability, basal friction, and roughness. In this first set of experiments, we assess the impact that reduced friction (increased sliding) at different locations (five zones) along the flowline has on ice discharge (Figure 1A). In all experiments we assume that the sliding parameter, A_s, represents changes in bed characteristics of any form, including roughness, permeability, or changes in the effective pressure. Numerically, sliding parameter A_s represents changes of the bed drag parameter AS and the effective pressure.

3.1.1 Instantaneous perturbation in basal sliding

We assess glacier response to an instantaneous, 15-year long, perturbation by reducing the sliding coefficient by 20%, and then 80%, in each zone, one at a time (Figure 1B). While an 80% step-wise decrease in friction is probably unrealistic, this extreme adjustment allows us to assess a likely upper-bound of glacier response. We repeat all experiments with a 3 and 6 month episodic perturbation to test how short-lived (seasonal) perturbations impact annual thinning and retreat.

Not surprisingly, a decrease in basal friction causes the glacier to accelerate and thin in the zone where the perturbation is applied and thicken down-glacier of the perturbation. The relationship between the sliding parameter (A_s) and discharge across the grounding line is not linear; a fourfold increase in discharge is not observed when the sliding parameter increases from 20% to 80%. When the perturbation is applied in zones 1-4, the region of thinning does not advect to the terminus within the 15-year experiment. Instead, because of the increase in ice velocity at these up-flow locations (zones 1-4), the terminus thickens. When the perturbation is applied to zone 5, close to the terminus, the glacier thins throughout the ablation zone and retreats (2 km for the 80% perturbation). The thinning extends 70-100 km up-flow, with a short time-lag of 6 months. Our results show that the time lag between the applied perturbation and the resulting acceleration depends largely on the location of the perturbation. When basal sliding is adjusted in zones 3-5 (closer to the terminus), the glacier accelerates immediately after the perturbation is applied, but quickly decelerates (within 1 year). When basal sliding is adjusted in zones 1-3, the acceleration

is delayed by 6 - 12 months and the subsequent deceleration lags by at least 12 months.

In all of the basal sliding experiments, we record only a small change in the terminus position (< 2 km) and an even smaller change in the grounding line position (< 1 km). As the glacier advances and retreats throughout the experiment, the velocity undergoes a concomitant acceleration and deceleration. This effect becomes less pronounced during the experiment as the glacier approaches a new equilibrium in 8-10 years.

Repeating the sliding experiments for a 6 month episodic perturbation (as opposed to an instantaneous and sustained one) yields similar results as the 15-year prolonged perturbation. However, if the same perturbation is applied for only 3 months at a time, the perturbation is not sustained and the glacier returns to its initial condition once the perturbation is removed.

3.1.2. Variable perturbations in basal sliding

In the variable perturbation experiments, we automatically adjust the sliding parameter A_s, both spatially and temporally, to constrain Helheim Glacier's discharge to match the observations in Figure 2. An infinite number of adjustments to the sliding coefficient can be made that mimic the observed velocity of Helheim Glacier. However, not all are physically reasonable. We limit our adjustments to the last 25 km of the glacier, which encompass zones 2-5, and ensure that the magnitude of change does not exceed 100%. Each scenario uniquely adjusts the rate at which the sliding parameter, A_s, changes in each zone. For example, in one scenario we set a maximum annual rate of change of 25% for each zone (Figure 3D), and in another a maximum rate of 60% only for zones 4 and 5, and less than 40% for the others (Figure 3F). In the absence of observations of how the sliding coefficient varies over time, we test a variety of different limits. Here, we present five of the possible scenarios in Figure 3. In each scenario, the model successfully mimics Helheim Glacier's discharge, but fails to reproduce the terminus evolution (Figure 4).

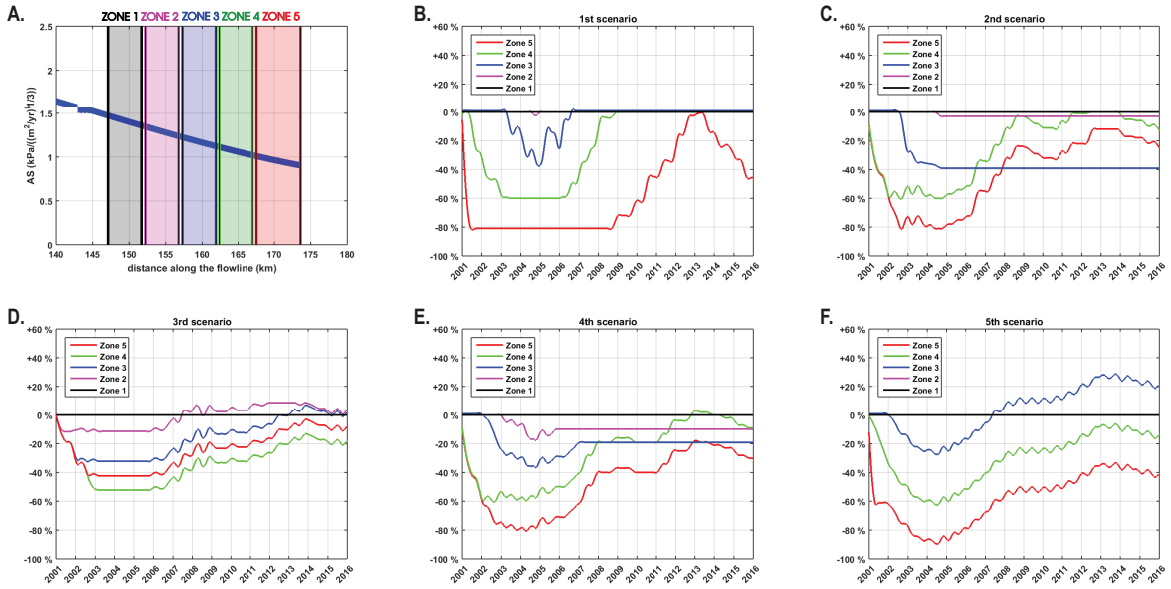

Figure 3: A) The sliding coefficient (A_s, blue line) for each zone that is used for the steady state model runs. Potential scenarios (panels B-F) of A_s values needed to obtain the observed discharge of Helheim Glacier. The adjustments to A_s are based on % change from the steady state values.

3.2 EXPERIMENT #2: INCREASED CALVING

At the termini of tidewater glaciers, iceberg calving can remove large volumes of ice over short time periods. Glacier retreat takes place when calving occurs at a rate that is faster than the terminus ice velocity. Calving processes are difficult to parameterize in glacier flow models because they depend on a number of poorly constrained variables (crevasse depth, amount of water in crevasses) that are used to mimic complex calving processes. We use the full crevasse calving criterion from Nick et al. (2010) that adjusts the terminus position based on terminus ice thickness and the penetration of surface and basal crevasses. Because water-filled crevasses more readily penetrate through ice, this criterion is very sensitive to the depth of water inside surface crevasses (Cook et al., 2014; Nick et al., 2010). The experiments in this section assess the impact of calving on Helheim Glacier's flow behavior. We control the calving rate by adjusting the amount of water in surface crevasses at the terminus. We conduct two types of perturbations: instantaneous experiments to test the sensitivity of our updated calving criterion, and variable, to evaluate the results using observational data from Helheim Glacier (Figure 2).

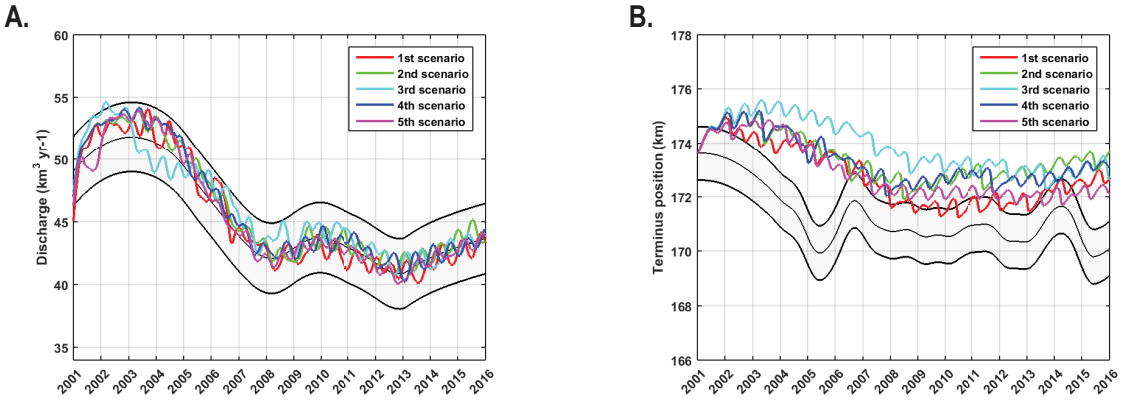

Figure 4: A) Discharge across the grounding line between 2001-2016, using a variable sliding coefficient as shown in the scenarios in Figure 3. B) Terminus position change for each scenario.

3.2.1 Instantaneous perturbation in calving

We use both the original crevasse criterion (Nick et al., 2010) and our modified criterion (Section 2.2) to assess the impact of instantaneous retreat on ice discharge. As such, the depth of water in crevasses is parameterized three different ways: uniformly (original criterion), increasing linearly from the ELA to the terminus, and increasing non-linearly from the ELA to the terminus (Figure 5A). Instantaneous retreat is achieved by increasing the water-depth in surface crevasses by 20% (Figure 5B) and 60%. In these experiments the penetration of the surface crevasses that initiate far from the terminus is set to zero.

In all experiments, a 20% increase in crevasse-water depth is sufficient to cause instant retreat. When the distribution of water along the glacier trunk is constant (blue line, Figure 5), the glacier retreats 5 km and loses the majority of its floating tongue. Retreat is reduced when water in crevasses increases linearly (red line, Figure 5) or exponentially (green line, Figure 5) from the ELA to the terminus. Larger patterns of retreat are found in all cases when the water depth increases by 60%. Regardless of the calving criterion parameterization, the terminus position restabilizes in the first two years, even though the step-wise perturbation persists for 15 years. In all experiments, retreat causes thinning that can extend up to 100 km up-flow after 15 years. Larger retreats cause enhanced thinning within the first 10 years, but all experiments have similar thinning rates after 10 years, regardless of the amount of retreat. When a spatially uniform crevasse

water depth is used throughout the ablation zone, the flowline model is very sensitive to the water in crevasses (blue line, Figure 5B), a result also found by Nick et al. (2010).

Our modified crevasse-water distributions have a smaller impact on discharge than the original calving criterion, yet it is still able to mimic seasonal ice velocity and terminus length. When the model is run for more than 10000 years, we find that with or without our modification, the grounding line location does not change, and the model maintains a floating ice tongue.

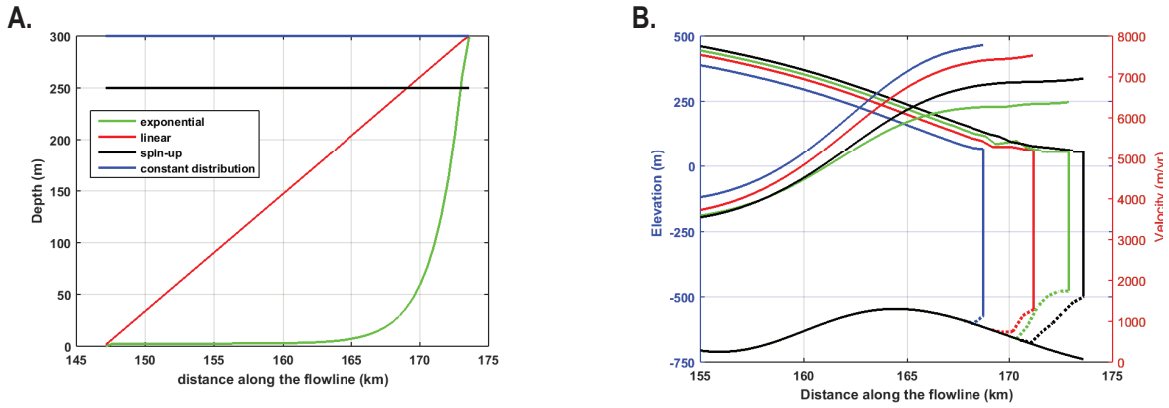

Figure 5: A) Water depth parameterizations used in our calving experiments. B) Glacier geometry and ice velocity results using the different water depth parameterizations shown in panel A (with corresponding colors), and an increase in water depth of 20% from the spin up results. The black lines represent results from the model spin up using a uniform water depth.

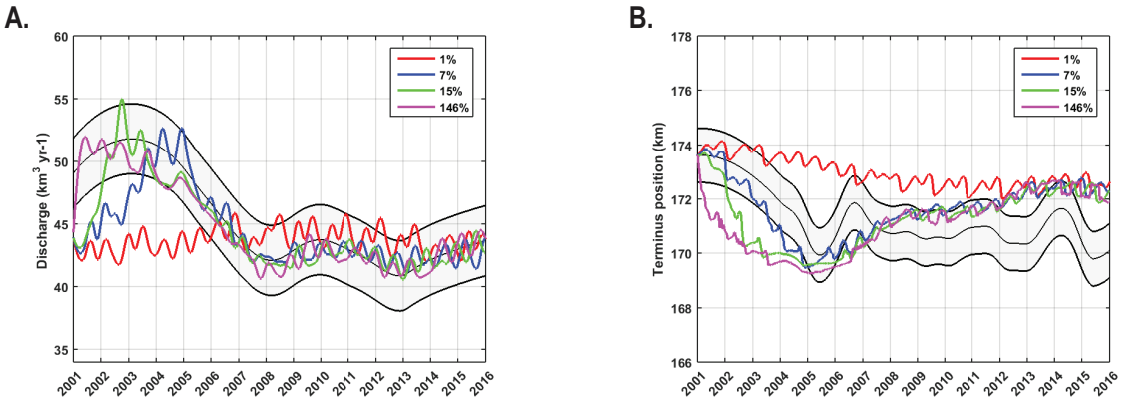

Figure 6: A) Observed (grey shading) and modeled (colored lines) discharge from 2001 to 2016. We constrain the rate at which water level can change in each scenario: 3.65 m yr^{-1}, 18.25 m yr^{-1}, 36.50 m yr^{-1}, and 365.0 m yr^{-1} (corresponding to 1%, 7%, 15% and 146%, respectively), B) Terminus position change for each water-depth scenario.

3.2.2 Variable perturbations in calving

We introduce a variable perturbation in calving by adjusting the water level in crevasses at each time step so that the modeled outputs match the observations in Figure 2. Because there are no observations of crevasse water depth to constrain our model experiments, we focus on the rate of water depth change, which is easier to put likely realistic constraints on. While there are many potential scenarios that could meet the discharge criteria, we show results from four scenarios. The scenarios are constrained by a crevasse water depth rate of change of 3.65 m yr^{-1}, 18.25 m yr^{-1}, 36.50 m yr^{-1}, and 365.00 m yr^{-1} (corresponding to 1%, 7%, 15% and 146% change, respectively). While the latter constraints are probably unrealistic extremes, they are useful in showing the range of perturbation necessary to match the observations. Results of the variable perturbation show that the observed discharge cannot be matched using the most realistic rate of water-filled crevasse depth change (3.65 m yr^{-1}, Figure 6A). Only the most extreme and unrealistic rate of change in crevasse water depth (365.00 m yr^{-1}) can match the discharge observations; all the scenarios fail to reproduce the terminus evolution (Figure 6B), since the terminus seems to respond too slowly to calving adjustments.

3.3 EXPERIMENT #3: REDUCTION IN BACKSTRESS

One proposed mechanism for tidewater glacier instability states that a reduction in pro-glacial mélange decreases backstress at the terminus and causes the glacier to calve and retreat (Amundson et al., 2008). However, the role of the mélange is complicated by the fact that it is composed of icebergs, which are a product of the calving process. When there are more icebergs in the fjord, the backstress will increase (due to a thicker or more rigid mélange) and the longitudinal stress at the terminus will decrease (equation 2), causing the glacier to decelerate, advance, and generate fewer icebergs. As a result, the mélange will weaken and thin, reducing the backstress, and causing acceleration and retreat. This negative feedback may play an important role in modulating terminus behavior.

In our study we conduct a series of experiments to test the role of backstress on terminus dynamics. However, the amount of backstress that a proglacial mélange applies to a glacier terminus is not easily quantifiable. We use a value of 15 kPa, which is likely an over-estimate of the actual value for Helheim Glacier. Numerically, a distribution of backstress along the flowline, $\sigma_b(x)$, impacts the second boundary condition of the force balance equation (equation 2).

We incorporate the mélange feedback effect by adjusting the backstress pressure as the glacier retreats. We use a linear distribution of backstress, with a minimum at the original terminus location. All experiments are run for 15 years and use a linear distribution of water-filled crevasses (Section 2.2).

3.3.1 Instantaneous reduction in backstress

We experiment with a sudden perturbation that reduces the backstress by 15%. Without including the feedback process described above, a reduction in backstress causes the glacier to increase discharge by 2.5% and retreat by 2 km. When we incorporate the feedback effect, retreat is reduced to 1 km and the increase in discharge is 1.5%. In both cases, the glacier stabilizes to a new position within 2 years.

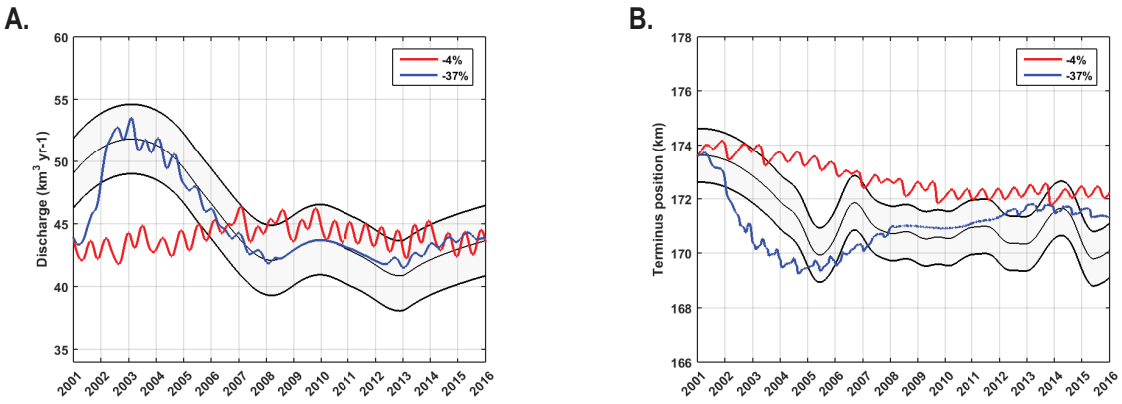

Figure 7: A) Observed (grey shading) and modeled (red and blue lines) discharge from 2001 to 2016. We assess the effect that mélange backstress has on discharge by constraining the rate at which the backstress can change in each modeling scenario: -4 kPa yr^{-1} and -37 kPa yr^{-1} (corresponding to -4%, and -37%, respectively). B) Terminus position change for each scenario.

3.3.2 Variable perturbations in backstress

Similar to variable perturbations applied in other experiments, we iteratively adjust the backstress at each time step in an attempt to match the observed discharge of Helheim Glacier. We test two perturbations: -4 kPa yr^{-1} and -37 kPa yr^{-1} (corresponding to -4%, and -37%, respectively). Our results show that we can only simulate Helheim Glacier's large increase in discharge from 2002 to 2005 (Figure 7A), by applying (physically impossible) negative values of backstress that reach -50 kPa in the second year of our experiment. Both experiments fail to reproduce the terminus evolution (Figure 7B).

3.4 EXPERIMENT #4: INCREASE IN SUBMARINE MELTING

Enhanced submarine melting at the terminus can cause thinning and retreat (Rignot et al., 2010). Submarine melt rates can vary due to fjord circulation patterns, water temperatures, and subglacial plume dynamics (Sciascia et al., 2013; Sutherland et al., 2014). For glaciers in West Greenland, Rignot et al. (2010) estimate the submarine melt rate to be between 255 m yr^{-1} and 1423 m yr^{-1}. In this study we use 580 m yr^{-1} for Helheim Glacier (Sutherland & Straneo, 2012) for our steady state run, and investigate how a change in subglacial melting could affect flow behavior. In our submarine melting experiments, we conduct experiments both with and without the backstress feedback effect described in Section 3.3.1.

3.4.1 Instantaneous increase in submarine melting

We use a linear approximation to set the submarine melt rate to zero at the grounding line and a maximum value 1 km away (Sciascia et al., 2013; Slater et al., 2017). To initiate the perturbation, we instantaneously alter the maximum melt rate by 20% and leave it elevated for 15 years. Because the impact on glacier geometry and discharge after 15 years is minimal (less than 3%), we repeat the experiment with a submarine melt rate of 870 m yr^{-1} (corresponding to a 50% increase), and assess the impact on discharge and terminus position with and without the backstress feedback

effect. A 50% increase in submarine melt rate causes a small acceleration (15%) and retreat (2.5 km) after 15 years. When we enable the backstress feedback effect during the retreat, the glacier accelerates only 3% and retreats 1 km, and we record 30% less thinning.

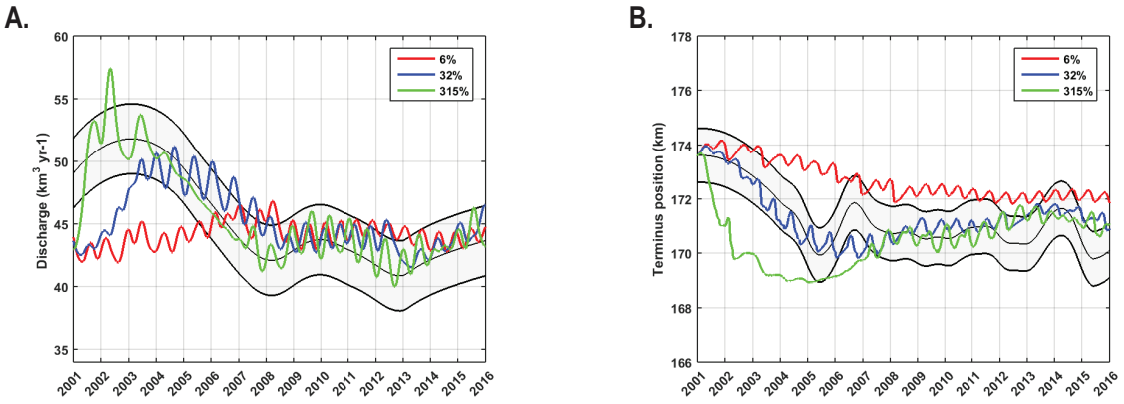

Figure 8: A) Observed (grey shading) and modeled (colored lines) discharge from 2001 to 2016. We assess the effect that submarine melt rate has on discharge and terminus position by constraining the rate at which melt can change over time: 36.5 m yr^{-1}, 182.5 m yr^{-1}, and 1825 m yr^{-1} (corresponding to +6 % or +32 % or +315 %, respectively). B) Terminus position change for each scenario compared with observations.

3.4.2 Variable increase in submarine melting

We apply variable adjustments in submarine melting at each time step in an attempt to simulate Helheim Glacier's dynamic behavior between 2001 and 2016. As in the other variable perturbations, we create model scenarios using a few different rates of change, in this case: 36.5 m yr^{-1}, 182.5 m yr^{-1}, and 1825.0 m yr^{-1} (corresponding to +6% or +32 % or +315 %, respectively). While an 1825.0 m yr^{-1} increase in submarine melting is very high, it is the only scenario that can match Helheim Glacier's pattern of discharge (Figure 8A). All the experiments fail to reproduce the terminus evolution (Figure 8B).

4.0 DISCUSSION

Whether processes at the ice-ocean or the ice-bed interface modulate Helheim Glacier's large-scale dynamics has been investigated for over a decade, with observations and models that seem

to support both (Nick et al., 2009; Nick et al., 2013; Bevan et al., 2015). While a change in basal processes was likely needed for Helheim Glacier to accelerate in 2002 – 2005, the question is whether additional melt water or a change in geometry (due to large-scale retreat) initiated the acceleration. And, conversely, whether the observed deceleration in 2006 was driven by a reduction in basal melt or terminus dynamics.

Despite using fundamentally the same flowline model, we conclude that basal sliding controls Helheim Glacier's behavior, while Nick et al. (2009) conclude that terminus dynamics control the behavior. An important distinction between our experiments and those in Nick et al. (2009) is the treatment of the terminus position and the grounding line. Nick et al. (2009) make the assumption that the grounding line retreated ~7 km between 2003 and 2005, and don't consider a floating portion. In our model, we make the assumption that the grounding line did not change, but that the floating tongue retreated by ~5 km between 2003 and 2005. This assumption is based on observations of tidal height from GPS receivers in 2005-2010 (Leigh A. Stearns, unpublished data) and radar echograms in 2001 and 2010 (Leuschen & Allen, 2011). As a result, while our model yields similar results as those in Nick et al. (2009), our interpretations are quite different. We conclude that an increase in basal sliding caused an increase in ice discharge (acceleration and thinning), and an increase in surface water in crevasses led to the retreat of Helheim Glacier's floating tongue. Throughout all of these changes the grounding line was stationary. Nick et al. (2009) conclude that, because basal sliding did not cause a ~7 km retreat of the grounding line, it is not an important perturbation.

Our modeling experiments show that only a change in basal sliding can reproduce Helheim Glacier's acceleration and subsequent deceleration. Parameters that alter calving rates (crevasse water-depth, mélange strength, submarine melt rates) are unable to mimic the velocity change and associated mass loss. While enhanced calving rates cause retreat, the subsequent thinning and acceleration in our model results are not large enough, nor do they occur quickly enough, to match observations. Consequently, our modeling results imply that there is a close relationship between surface melt and basal lubrication near the terminus, and that basal lubrication can undergo large

changes over short time periods.

Observations show that on short-time scales (diurnal), surface melt and ice velocity are tightly linked, implying first that surface melt can get to the bed of Helheim Glacier, and second that the additional water lubricates the ice-bed interface. Using co-located GPS and weather station data, Andersen et al. (2010) record a significant correlation (>95%) between variations in surface melt and ice velocity near the terminus. Similarly, Davis et al. (2013) observe diurnal-scale accelerations in their Helheim Glacier GPS network which they hypothesize are due to variations in basal lubrication from diurnal peaks in solar heating.

On other glaciers, borehole measurements further highlight the connection between changes in basal water pressure and ice velocity. In Patagonia, small diurnal changes (3-5%) in basal water pressure are correlated with large changes (40%) in ice velocity (Sugiyama et al., 2011). In Switzerland, diurnal changes in water pressure exceed 100% and are correlated with rapid changes in ice velocity (Iken & Bindschadler, 1986). Large swings in basal water pressure are also observed in boreholes in West Greenland (Thomsen & Olesen, 1991; Meierbachtol et al., 2013). In our experiments, we adjust the basal sliding coefficient, A_s, to achieve the observed ice velocity of Helheim Glacier from 2001 – 2016. Our parameterization of the diurnal changes in basal sliding A_s, and the corresponding basal drag, appears to be within the bounds of the observations listed above. These diurnal variations in flow speed and basal sliding support our parameterizations in Section 3.1.2, where basal sliding is adjusted at every time step (0.0027 years) in variable perturbation model.

Our results suggest that only crevasse water depth can reproduce Helheim Glacier's terminus behavior. This finding mimics other modeling results for Helheim Glacier (e.g. Nick et al., 2009; Cook et al., 2014). In particular, Cook et al. (2014) also assessed the sensitivity of the terminus position to basal water pressure, submarine melt rates, mélange rigidity and crevasse water depth and reached the same conclusion. Terminus position was most sensitive to changes in crevasse water depth.

Because there are no long-term measurements of crevasse water depth, observational studies

assess terminus sensitivity by correlating time-series of air or ocean temperatures to terminus position. Several studies show that Helheim Glacier retreated when air temperatures were higher than usual (2002 – 2005), and re-advanced during subsequent cooler periods (Joughin et al., 2008; Khan et al., 2014). Similarly, for neighboring Kangerludssuaq Glacier, observational data suggests that air temperatures play a larger role in retreat patterns than ocean temperatures, despite the fact that fjord temperatures are higher than at Helheim Glacier (Christoffersen et al., 2011; Christoffersen et al., 2012).

Since mechanisms are not independent from each other, we conduct a final experiment that uses a combination of atmospheric-driven perturbations to simulate Helheim Glacier's behavior from 2001 to 2016. We apply variable perturbations in basal sliding and crevasse water depth at every time step so that the model outputs are similar to the observations for ice discharge and terminus position (Figure 2A, B). The model results show that we can successfully mimic the ice discharge and terminus evolution of Helheim Glacier using realistic changes in these parameters (Figure 9). No other combination of realistic variable perturbations can successfully mimic Helheim Glacier's complex behavior during this time period.

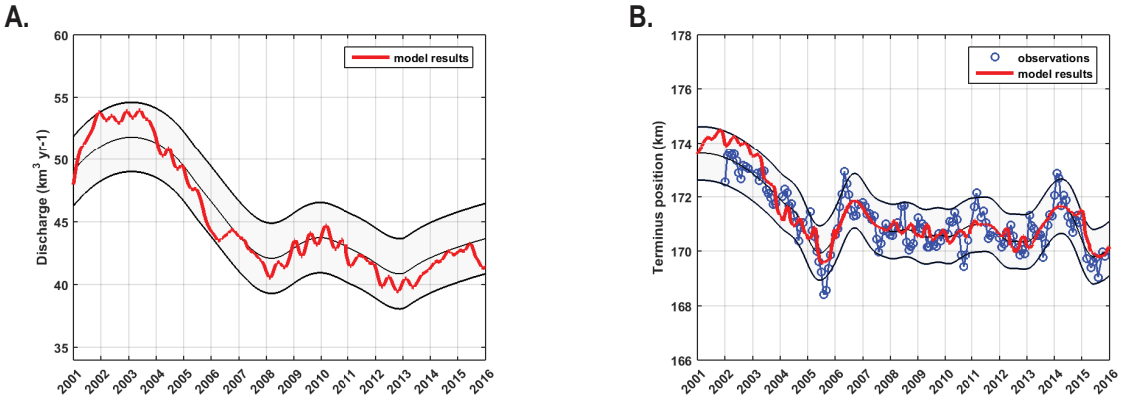

Figure 9: A) Observed (grey shading) and modeled (red line) ice discharge using the combined atmospheric forcings. B) Observed (blue dots and grey shading) and modeled (red line) terminus position using the combined atmospheric forcings.

The model results in Figure 9A and 9B are based on a scenario where basal sliding is only adjusted in the last 23 km of Helheim Glacier (zones 2 – 5). However, we also create a series of scenarios that match the observations and are based on the diurnal percent change of basal sliding

in each zone. These adjustments to the sliding parameter are generally small. However, during the large acceleration beginning in 2001, basal sliding near the terminus changes by 30%, comparable to the percent change in terminus ice velocity. Similarly, water depth in crevasses changes by a maximum rate of 7% each year, except during the large-scale retreat in 2005 when it changes by 15%. This large increase in water depth may be reasonable given the combined effect of warmer air temperatures (Joughin et al., 2008) and increased stretching due to acceleration beginning in 2001. Between the summer of 2005 and the fall of 2006 when the glacier advanced by more than 3 km, our model suggests that water depth in crevasses could have decreased by 25%. This advance was likely the combined result of decreased water in crevasses, possibly triggered by low 2006 summer temperatures (Joughin et al., 2008), and a linear distribution of crevasse water depth as described in Section 2.2.

Our final model, adjusting both sliding and crevasse water depth, reproduces two important characteristics of Helheim Glacier's behavior from 2001-2016. First, terminus retreat did not impact the location of the grounding line. Repeat radar echograms from 2001 and 2010 show that the grounding line at Helheim Glacier did not change substantially, despite large-scale retreat, thinning and acceleration (Leuschen & Allen, 2011). Second, the acceleration and thinning beginning in 2001 were not isolated to the terminus, but impacted Helheim Glacier at least 60 km up-flow of the terminus (Stearns et al., 2008). Our model results are consistent with this observation.

On long time-scales (decadal), it is more difficult to separate oceanic- and atmospheric-driven processes largely because of data availability. However using modeled runoff, Murray et al. (2010) show that Helheim Glacier's acceleration in 2003 occurred during a time of low runoff (average air temperatures were warmer, but the preceding winter's snowfall was low). Ocean mooring data, however, show anomalously warm temperatures in 2003. They conclude, therefore, that ocean processes drive Helheim Glacier's dynamics (Murray et al., 2010). Our modeling results contradict this conclusion; we cannot achieve the observed acceleration, which extends 50 km upflow from the terminus, with ocean forcings alone."

5.0 CONCLUSIONS

In this study we use a one-dimensional flowline model to assess whether predominantly atmospheric or oceanic forcings drove the changes in ice flow observed on Helheim Glacier, East Greenland from 2001 to 2011. In particular, we investigate if the large-scale dynamic changes observed on Helheim, could be triggered exclusively by processes at the terminus or along the glacier trunk. We show that both forcings can influence glacier behavior, but changes associated with the ice-bed interface result in larger and more long-lived changes to ice discharge than changes at the ice-ocean interface.

Chapter 2: Importance of geometry in providing stability to Greenland glaciers undergoing decadal-scale retreat

1.0 INTRODUCTION

Over the past two decades, ice discharge from the Greenland Ice Sheet (GrIS) increased twofold due to changes in climate (Rignot et al., 2011b; van den Broeke et al., 2016). However, the mechanisms driving the increased discharge, and the features that modulate glacier response, are not well understood. In particular, neighboring glaciers, which are likely subject to similar climate forcings, have responded very differently to those forcings (e.g. Bartholomaus et al., 2016; Motyka et al., 2017).

Overall, Greenland tidewater glaciers are retreating (Moon et al., 2012), but the rate, magnitude, and timing of retreat varies greatly, even between adjacent glaciers. An example of this is the asynchronous retreat of glaciers in southeast (Howat et al., 2008) and southwest (Truffer & Motyka, 2016) Greenland. Glacier flow variability, at least on seasonal scales, is likely dictated by whether a glacier is more sensitive to perturbations at the ice-bed or ice-ocean interface (Moon et al., 2012, 2014). However, it remains unclear as to what causes a glacier to be more sensitive to one perturbation rather than another. Therefore, one common hypothesis is that while variations in atmospheric and oceanic forcings likely trigger the acceleration and retreat of tidewater glaciers, how a glacier responds to these forcings is dictated by individual glacier geometry and basal condition (e.g. Enderlin et al., 2012).

Glacier geometry, particularly glacier width and bed slope near the terminus, has been proposed as the dominant variable controlling the rate at which a tidewater glacier retreats (Enderlin et al., 2012; Carr et al., 2015; Durkin et al., 2017). Resistance to glacier flow comes from friction at the lateral margins and ice-bed interface, therefore the geometry of these margins could modulate glacier response during retreat (Pfeffer, 2007), especially if the glacier retreats into a narrower or shallower region. In fact, a prevailing glaciological theory is that grounding lines located on reverse bed slopes are inherently unstable (Hughes, 1981; Schoof, 2007). However, models that include lateral drag can have grounding lines that are stable regardless of the bed slope (O'Neel et al., 2005; Pfeffer, 2007; Gudmundsson et al., 2012; Jamieson et al., 2012).

Given the complex and interconnected physical processes controlling tidewater glacier dynamics, isolating the role of glacier geometry is difficult given observational data alone. Instead, numerical models are needed to investigate whether geometry controls the sensitivity of Greenland tidewater glaciers to climate perturbations. In our study, we use a one dimensional flowline model to assess whether introducing bed and width variations near the terminus has an impact on a glacier's response to identical environmental perturbations.

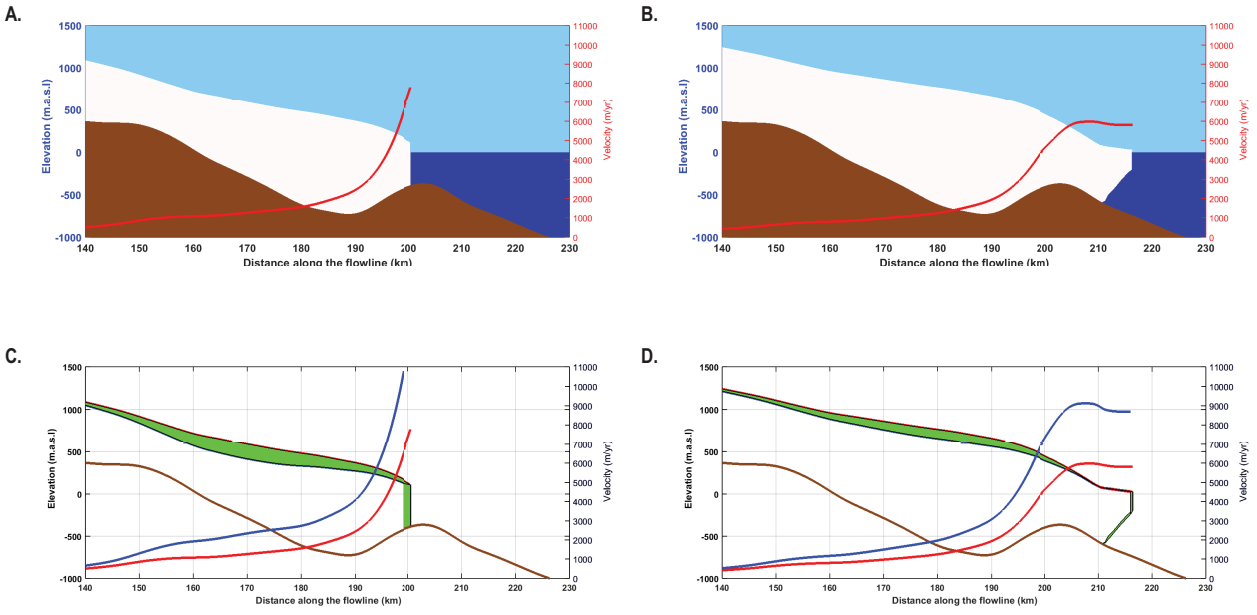

Figure 10: Steady state conditions when the glacier stabilizes in (A.) a negative and (B.) a positive bed slope. We show the initial and final geometry and ice velocity for the steady state profiles of (C.) a negative and (D.) a positive bed slope after a 10 year perturbation is applied. The green shading highlights the amount of thinning after 10 years.

2.0 METHODS

We use a one-dimensional, width-averaged, depth-integrated, full stress flow-band model (Petrakopoulos et al., in preparation) to assess the role of glacier geometry in modulating glacier retreat patterns. In particular, we explore the relative role of bed topography and glacier width in dictating how a glacier undergoes retreat. As such, we create two steady state glacier geometries

– one with a negative bed slope and one with a positive bed slope (Figure 10A, 10B). We apply an instantaneous perturbation to both bed slope profiles and quantify how the profiles evolve over 10 years. We then slightly modify the geometry of the two initial bed slopes and assess how they respond to the same instantaneous perturbation. Through this method, we isolate the role that geometry plays on glacier behavior.

2.1 Numerical model

Our numerical flowline model (Petrakopoulos et al., in preparation) is similar to flowline models used in other studies (Nick et al., 2010; Enderlin et al., 2013; Carr et al., 2015). The model relies on the conservation of momentum equation Nick et al. (2010):

$$-(AS)\,[(H-\frac{\rho_w}{\rho_i}\ |H_{base}|)\,U]^{\frac{1}{3}}-2\frac{H}{W_{full}}\,(\frac{5U}{AW_{full}})^{\frac{1}{3}}+2\{\frac{\partial}{\partial x}[HA^{-\frac{1}{3}}|\frac{\partial U}{\partial x}|^{-\frac{2}{3}}\frac{\partial U}{\partial x}]\}=\rho_i\,g\,H\,(\frac{\partial H_s}{\partial x})\ , \tag{7}$$

and the depth-integrated continuity equation (van der Veen, 2013):

$$\frac{\partial H}{\partial t}=-(\frac{1}{W_{full}})\frac{\partial(H\,U\,W_{full})}{\partial x}+S\dot{M}B+\dot{m}_{float}\ , \tag{8}$$

where ρ_i is the ice density (917 kg m^{-3}), ρ_w is the ocean water density (1025 kg m^{-3}), and g is the gravitational acceleration (9.806 m s^{-2}). The distance along the flowline is x, H is the thickness of the glacier, H_{base} is the bed elevation (negative below sea level), W_{full} is the glacier width, H_s is the surface elevation, and U is the depth-integrated, width-averaged ice velocity. For the basal drag, the parameter AS, is fixed, and the exponent of the sliding relation, m, is set to 3. Numerically, the changes of the AS and the effective pressure expressed by the changes in sliding parameter A_s. For stability reasons, the time step is small (0.0027 years), which allows us to assume zero acceleration between epochs. We use an exponent, n, of 3 in Glen's flow law, and set the rate factor, A, to 3.5 10^{-25} s^{-1} Pa^{-3} which is equivalent to an ice temperature of -10°C (Cuffey & Paterson, 2010). $S\dot{M}B$ is the surface mass balance (SMB) rate, and $\dot{m}_{float}$ is the submarine melting rate, if a floating tongue exists. We use a modified calving criterion, where the water depth inside surface crevasses

increases linearly from the ELA to the terminus (Petrakopoulos et al., in preparation). All of the experiments use a modified Weertman sliding relation (Kamb, 1987). We do not incorporate any ice mélange pressure at the calving front in these experiments. Each model experiment runs until it satisfies a steady state condition or reaches the maximum of 10 years.

Table 1: List of the 15 studied glaciers

Alison Glacier	Rink Isbrae
Deception 0 (unnamed)	Sermeq Silarleq Glacier
Hayes Glacier	Store Glacier
Helheim Glacier	Sverdrup Glacier
Illullip Sermia	Upernavik Isstrom Central
Jakobshavn Isbrae	Upernavik Isstrom North
Kakivfaat Sermiat	Uunartit Islands (unnamed)
Kong Oscar	

2.2 Model Setup

Our experiments start with two steady state glacier profiles – one with a negative slope (Figure 10A), and one with a positive slope (Figure 10B). In an effort to use realistic profiles of Greenland glaciers, we base the geometry (bed, width, and ice thickness) and boundary conditions (surface mass balance and submarine melt rates) on 15 glaciers that have high rates of discharge as well as relatively smooth, well characterized beds (Morlighem et al., 2014; Noël et al., 2015; Rignot et al., 2015). These glaciers are shown in Figure 10 and are listed in Table 1. A linear least squares regression is applied to the mass-conserving bed topography (Morlighem et al., 2014) of the 15 glaciers to create two steady state bed profiles; one with a positive slope and one with a negative slope.

We make minor geometry modifications to the two steady state profiles in order to run our experiments on a range of geometries that are typical of Greenland glaciers. We make changes to

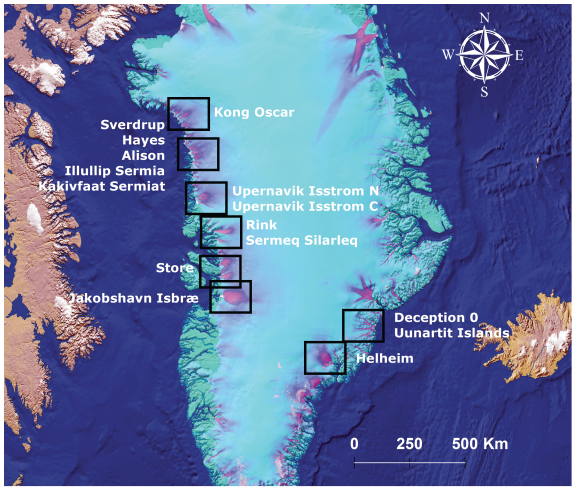

Figure 11: The location of the 15 glaciers used in this study, overlain on a Greenland velocity map Rignot & Mouginot (2012).

the bed topography by adding subglacial highs and lows at different locations along the profile, and changes in width by adding narrow and wide sections along the profile. In all, we create 46 steady state profiles divided into two categories – those with a positive bed slope, and those with a negative bed slope. The glacier geometries used in this study, all of which are loosely based on real glaciers, are shown in Figures 12A, B and 13A, B.

We conduct experiments on all 46 glacier profiles (the two initial profiles and the 44 modified ones). Before we add any perturbations, we get the 46 profiles to steady state condition, which is the result of a 10,000 – 100,000 year spin up, or until no significant oscillation of any variable is recorded. Model variables, including the sliding parameter A_s, crevasse water depth, surface mass balance, and submarine melt rate are the same for all steady state model runs. To constrain the surface mass balance (SMB), we use annual RACMO 2.3 data from 2010 to 2015 at 1 km resolution (Noël et al., 2015), extracted along the centerline of the 15 glaciers on which our profile is based. We use a maximum submarine melt rate of -650 m yr^{-1}, one kilometer seaward of the terminus (Sciascia et al., 2013; Slater et al., 2017). In steady state, all 46 profiles yield similar discharge values and terminate within 0.5 km of the same location.

3.0 EXPERIMENTS

To determine whether glacier behavior is controlled by local variations in bed topography and width impact retreat behavior, we apply the same instantaneous perturbation to all 46 glacier profiles. The perturbation consists of a 20% increase in submarine melting, a 30% increase of water in surface crevasses at the terminus, and an increase in basal sliding. We increase basal sliding incrementally along the flowline; 50% at a distance of 7-14 km from the grounding line (zone 1, Figure 12), and 90% at a distance of 0-7 km from the grounding line (zone 2, Figure 12). For each experiment we record the final geometry and the discharge at the grounding line.

3.1 Experiment #1: Bed variations

Our first set of experiments is based on profiles with modified bed topography in the ablation zone. As described in Section 2.2, bed variations are based on the characteristics (height, length, and distance from grounding line) of 15 fast-flowing glaciers in Greenland (Figure 11). Bed modifications are added to both steady state profiles – those with a positive slope and those with a negative slope near the grounding line. Nine bed modifications are added to the steady state profile with the negative bed slope and 21 bed modifications are added to the steady state profile with the positive bed slope. We classify the bed modifications by their distance from the grounding line (zones 1, 2, and 3 in Figure 12). In steady state, nearly all profiles have the same grounding line location, but different surface elevation and ice velocity values. Steady state profiles ♯20 and ♯21, both variations with positive bed slopes, are unique because their grounding lines are located 2.5 km farther down-glacier than the other profiles. The instantaneous perturbation is applied to all profiles for 10 years.

Results of the negative bed slope profiles show that, compared to the initial steady state (Figure 12A, black line), profiles that are modified with topographic highs cause an increase in ice discharge after 10 years and profiles that are modified with topographic lows cause a reduction in discharge (Figure 12C). In all of the experimental runs on a negative bed slope, the change in dis-

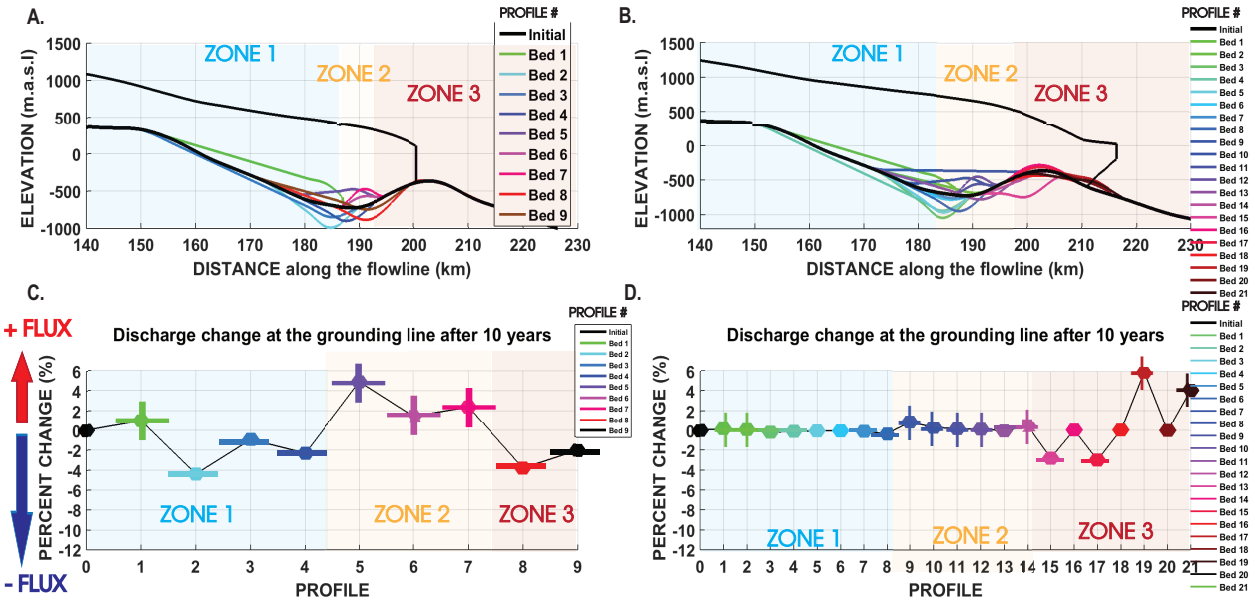

Figure 12: a). Nine modifications to the initial negatively-sloped bed topography (black line), separated by along-flow zone in negative (A) and positive (B) slope. b). Percent change in discharge for each bed profile relative to the initial topography, following a 10-year imposed retreat, in negative (C) and positive (D) slope. In panels C and D, the + and − signs identify bed highs (+) and lows (−) added to the profiles in panels A and B.

charge after 10 years does not exceed 5% (Figure 12C). All profiles lost mass due predominantly to glacier thinning, along with a small retreat (less than 2 km), and most of the mass loss occurred in the first 2-3 years. While thinning continues until the end of the experiment, it is at a much slower rate than the first 3 years. Within 10 years, all profiles reach a stable geometry; if the perturbation is removed, all glaciers return to their initial condition in less than 3 years.

For the most part, bed modifications to a positive bed slope have a negligible impact on discharge (Figure 12D). Only four profiles cause a variation in discharge compared to the initial steady state profile, all of which are within 10 km of the grounding line (Figure 12B). Two profiles that add bed highs in zone 3 cause an increase in ice discharge (Figure 12D), and two profiles that add bed lows in zone 3 cause a decrease in ice discharge (Figure 12D). However, these four profiles cause discharge variations that are less than 6% (Figure 12D). All profiles with a positive bed slope undergo thinning along the trunk, but sustain a fairly stable terminus for the first 5 years of the experiment. After 5 years, thinning along the glacier trunk advects to the terminus, initiating a

small retreat (less than 1 km). Mass loss at the grounding line is less than for profiles on a negative slope. As in the other experiments, if the perturbation is removed, all glacier profiles return to their initial condition in less than 3 years.

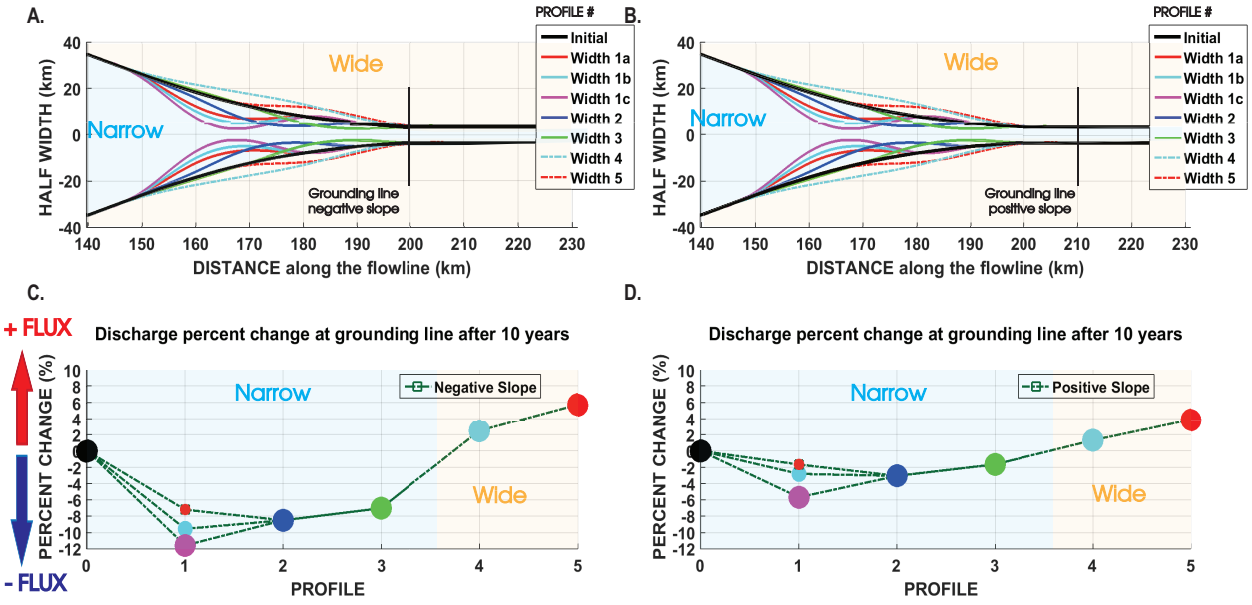

Figure 13: a). Five glacier width variations applied to a A) negative and B) positive bed slope. Profiles 1, 2, and 3 are narrower, and profiles 4 and 5 are wider than the initial width 0 (black line). b). Percent change in discharge after a 10-year perturbation for each width variation over a C) positive and D) negative bed slope.

3.2 Experiment #2: Width variations

In our second set of experiments we modify the glacier width in the ablation zone, and assess how different steady state profiles respond to the same instantaneous perturbation described in Section 3.0. As with the bed modifications, width variations are based on the characteristics of our 15 selected glaciers and added to positive and negative bed slopes (Figure 13A, B). Seven variations in width are made to the initial negative bed profile (Figure 13A) and seven variations in width are made to the initial positive bed profile (Figure 13B). The grounding line in all of the steady state profiles is in the same location, except for profile ♯3 (Figure 13B). Profile ♯3 modifies the positive bed profile by producing a very narrow region near the terminus where the glacier is

thickest (Figure 10B). In steady-state, the grounding line of profile ♯3 is 2 km more advanced than all the other profiles. Following the same instantaneous perturbation, all profiles (including profile ♯3) reach a stable geometry where retreat is less than 1 km. The results of width variations show that, compared to the initial steady state (Figure 13A, B, black line), narrower profiles reduce ice discharge from an imposed retreat after 10 years. Wider profiles cause an increase in ice discharge from the same imposed retreat after 10 years. A profile that is narrow near the ELA (profile 1a, Figure 13C, D) has a similar ice discharge after 10 years as a profile that is narrow near the terminus (profile 2, in Figure 13C, D). The change in mass loss with different widths on a negative slope does not exceed 12% (Figure 13C), and for profiles on a positive slope does not exceed 6% (Figure 13D). The largest increase in discharge occurs in the first 3 – 4 years for all profiles. In years 6 – 10, both terminus and grounding line position remain at the same location, and we record slow, but continuous, thinning. If we remove the perturbation, all glaciers return to the initial geometry in less than 3 years.

3.3 Experiment #3: Amplified forcing

In the previous experiments (Section 3.1 and 3.2), we use a linear distribution for water in surface crevasses (Petrakopoulos et al., in preparation) and the results show that none of the model glaciers retreat more than 2 km. In a last series of experiments, we apply the same perturbation, but we use a non-linear distribution of water in crevasses from the ELA to the terminus. This non-linear distribution acts to increase water penetration in crevasses by roughly 50% near the terminus, thus amplifying the initial perturbation. We conduct this experimental run on the same suite of bed topographies shown in Figure 12.

Despite a slightly larger retreat, ice discharge at the grounding line does not increase more than 20% of the initial profile. The largest changes in ice discharge are caused by profiles that add bed highs to the positive bed slope (Figure 12A, B) and widen the glacier margins (Figure 13A, B). Terminus retreat is larger than it was in the previous experiment (Section 3.2) - 5 km in the negative slope and 2 km in the positive slope. Glacier widening also causes enhanced retreat (5

km). However, we do not record an unstable retreat in any of these scenarios.

4.0 DISCUSSION

Stresses at the terminus of glaciers are controlled by glacier geometry (e.g. van der Veen & Whillans, 1996) and modeling studies largely conclude that topography near the terminus plays a key role in modulating glacier response to large-scale climate perturbations (e.g. Nick et al., 2007; Enderlin et al., 2012; Morlighem et al., 2016). Our model experiments, which include a modest climate perturbation over 10 years, also show that geometry dictates a glacier's response, even though the changes in terminus position and ice discharge are relatively small. In particular, our results show that fjord widenings and overdeepenings enable faster rates of retreat and enhanced ice discharge following a climate perturbation. This result is supported by observational studies of Alaskan glaciers, which are found to retreat quickly through basal overdeepenings and fjord widenings (Meier & Post, 1987; McNabb & Hock, 2014).

Other modeling studies impose an extremely large perturbation in order to achieve large changes in flow behavior (e.g. Nick et al., 2007; Enderlin et al., 2012; Morlighem et al., 2016). For example, Morlighem et al. (2016), show that an extremely large forcing (e.g. quadrupling the current submarine melt rate) is needed to initiate retreat of Store Glacier, West Greenland. However, once retreat begins, the magnitude of retreat is dictated by bed topography (Morlighem et al., 2016). In our study, when we parameterize surface water in crevasses using a linear distribution along the flowline, we get a maximum retreat of 2 km. However, when we amplify the calving criterion by using a different spatial distribution of water in crevasses, retreat increases to 5 km. As in the previous experiments, glaciers with grounding lines located on a negative slope or in a wider fjord undergo more retreat and acceleration.

In our study, we assume that all the glaciers start in steady state, which is not likely true for most glaciers in Greenland. Our results suggest that the contrasting behavior of so many neighboring glaciers in Greenland is the combined effect of the external forcing and glacier geometry. We find that the retreat of glaciers on negative slopes is not unconditionally unstable, in agreement with

studies by Gudmundsson et al. (2012). Over longer timescales (100 – 1000 years), surface mass balance plays a dominant factor in glacier length (Amundson & Truffer, 2010). The glaciers in all of our experiments return to their initial condition 2 – 3 years after the perturbation is removed. The latter finding indicates that those Greenland glaciers that thin and retreat for over a decade are likely to readvance and return to their initial condition following several years of a cooler climate. If the SMB does not change substantially, then the glacier should remain at its steady state geometry.

4.1 Bed Topography control

Many observational and theoretical studies show that as a grounding line retreats into deeper water, the discharge increases leading to a feedback that further accelerates retreat and subsequent discharge (e.g. Weertman, 1974; Thomas & Bentley, 1978 Meier & Post, 1987; Pfeffer, 2007; Schoof, 2007; Post et al., 2011; McNabb & Hock, 2014; Motyka et al., 2017). While our experiments do not trigger the irreversible retreat suggested in the above studies, we do find that the magnitude of retreat and ice discharge is larger for glaciers located on negative (reverse) bed slopes than those on positive bed slopes. Perturbations applied to glaciers with negative bed slopes usually result in thinner ice at the grounding line which, because of mass conservation, causes a large increase in ice discharge. This finding is largely consistent with the behavior of 32 glaciers in southeast Greenland between 2000 and 2006 (Howat et al., 2008), where those glaciers located on a negative slope retreated farther. Similar to our model results, all retreats were less than 5 km and occurred within a 4 year timespan.

In all experiments, we record continuous thinning during the 10 years of the perturbation; the magnitude of thinning relative to the ice thickness dictates whether there is a lag between the perturbation and subsequent retreat. On a negative bed slope, glacier retreat begins immediately after the perturbation is applied, coincident with thinning. With a positive slope, thinning also occurs immediately after the perturbation is applied, but retreat occurs 4 – 5 years later. This lag between thinning and retreat is caused by the thick ice that exists near the grounding line

of glaciers with a positive bed slope (see Figures 12A, B). It takes 4 – 5 years for these thicker termini to thin enough at the grounding line to undergo retreat. A similar lag has been observed on Columbia Glacier, which had a period of terminus stability despite undergoing several years of thinning before rapidly retreating through a negative bed slope (Meier & Post, 1987; O'Neel et al., 2005). Our modeling results support this pattern of events, but not such a large retreat due only to geometry. We hypothesize that both dynamic thinning and mass balance contributed to this behavior.

There are additional reasons why bed topography impacts how a glacier responds to ocean or atmospheric forcings. For example, in order for a glacier to be sensitive to atmospheric warming, water needs to collect in surface crevasses or penetrate to the glacier bed. The surface slope, longitudinal strain rates, and ice thickness will dictate whether these processes occur. Furthermore, in our model we assume that ocean warming will have the same impact on all glaciers. However, increased ocean temperatures will impact fjord circulation in different ways depending on the fjord bathymetry (e.g. Straneo et al., 2011). Similarly, the grounding line depth controls how effectively subglacial plumes can melt the terminus (Carroll et al., 2015). Overall, the complexity and interconnected nature of the mechanisms acting on glacier termini often masks the impact of bed topography on glacier stability.

4.2 Comparison with observations

In general, our modeling results show that glaciers are most stable on positive bed slopes and narrow sections of fjords. To assess whether this result fits with the behavior of Greenland glaciers, we investigate whether glaciers tend to stabilize in these geometries. Figure 14 shows that, for 75 glaciers around Greenland, the majority of them are currently located on either a positive bed slope or a narrow stretch of fjord. Very few glacier termini are located in both a fjord widening and negative bed slope. In Figure 14, we differentiate between termini located in the same position for several years and are likely in a stable geometry (triangles) with those that may not be in a stable geometry and only have one epoch in their retreated position (circles). The observation that bed

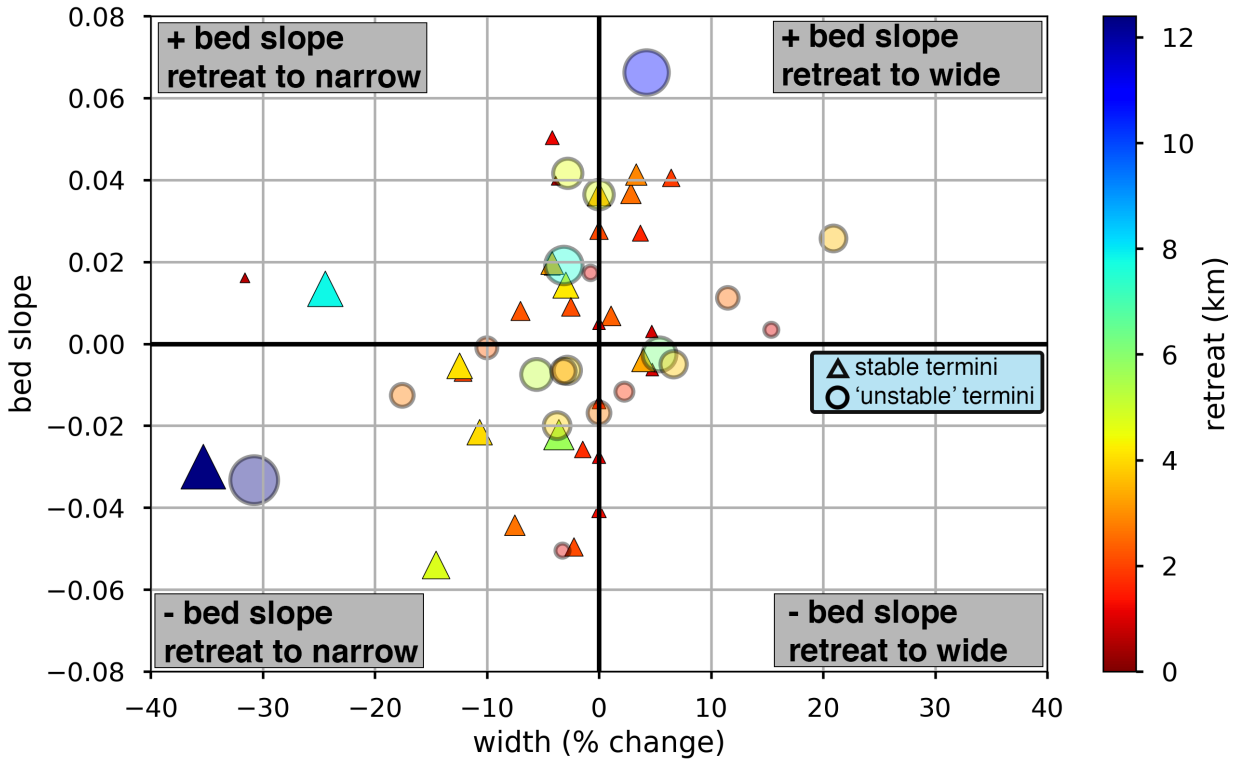

Figure 14: The relationship between glacier geometry and terminus position for 75 glaciers in Greenland. Bed slope is determined from the change in bed elevation (Morlighem et al., 2014) from the most terminal centerline position to 10 km up-flow. Percent width change is measured from a Greenland-wide optical image (Joughin et al., 2010b). Retreat magnitude is determined from Moon & Joughin (2015), using terminus position data from 2000/01 to 2012/13. Triangles represent stable termini positions (multiple years in the same position); circles represent potentially unstable termini positions (only one year at that position).

and width characteristics do temporarily stabilize glacier termini supports our overall conclusions. In addition, Figure 14 shows that the average retreat from 2000/01 – 2012/13 is 2.6 km. While three glaciers underwent large-scale retreats of 12 – 14 km, the majority of the Greenland glaciers underwent small-scale retreats similar to our model results.

5.0 CONCLUSIONS

Over the past two decades, Greenland glaciers have undergone large-scale, and disparate patterns of acceleration, thinning and retreat. Despite the fact that the mechanisms that control glacier

stability and instability are not well understood, some studies suggest that atmospheric and oceanic forcings are solely responsible for this behavior. However, adjacent glaciers respond differently to presumably similar environmental forcing, possibly due to differences in geometry. We show that both modulations in bed and width profiles play a small role in mass loss by a forced retreat that last 10 years. The narrow sections of a glacier, especially far from the glacier front, are the most effective at reducing glacier discharge and stabilizing retreat. Fluctuations in bed topography of neighbor glaciers are not important for ice mass loss.

Chapter 3: Paleo-grounding line evolution of Byrd Glacier from the Last Glacial Maximum to present

1.0 INTRODUCTION

The configuration of the Antarctic Ice Sheet is controlled by several different climate variables (e.g. surface mass balance, ocean circulation and temperature), which influence the ice sheet on different temporal and spatial scales. Identifying the mechanisms that drive the ice sheet's evolution, particularly retreat, is essential for understanding its present day stability and future behavior. While the present day ice sheet contains enough ice to raise sea level by 58 m (Pritchard et al., 2012), its retreat from its Last Glacial Maximum (LGM) position contributed up to 23 m to sea level (Clark et al., 2009). In this study, we model the potential climate variables that initiated retreat from the LGM position, along with intermittent points of stability during the prolonged retreat.

During the Last Glacial Maximum (26.5 –19 kya), the Antarctic Ice Sheet was at its maximum configuration, with grounded ice extending to the continental shelf in most places (Anderson et al., 2002; Clark et al., 2009; Bentley et al., 2014). During this time, air and ocean temperatures around Antarctica were likely 8°C colder, but began to rise starting around 19 kya (Jouzel et al., 2001; Morgan et al., 2002; Barrows et al., 2007; Anderson et al., 2009). As climate warmed, the ice sheet thinned and retreated. However, retreat patterns across the ice sheet were quite variable (Anderson et al., 2002), due to differences in climate forcing and local bed controls. Throughout the warming following the LGM, most of the Antarctic Ice Sheet's mass loss occurred in the Ross and Weddell Sea embayments (Denton & Hughes, 2002; Golledge et al., 2014; Pollard & DeConto, 2009). In the Ross Sea, grounded ice retreated more than 250 km from its LGM position to its current position.

In this study, we focus on retreat patterns through the Ross Sea along the Byrd Glacier flowline. Byrd Glacier is a major outlet glacier that drains ice from the East Antarctic Ice Sheet to the Ross Sea. During the last deglaciation, while Byrd Glacier retreated from the continental shelf to its current configuration, it left subglacial moraines on the sea floor (Anderson et al., 2014). Some of these moraines can be used as temporal indicators of grounding line stability. As a result, we can

use the moraines to reconstruct the retreat of Byrd Glacier from the LGM to present and assess the controls on the retreat. We use a one dimensional flowline model to investigate (i) whether atmospheric or oceanic forcings drove the retreat of Byrd Glacier; (ii) whether the Ross Ice Shelf existed throughout the retreat; and, (iii) how Byrd Glacier behaved after surface temperatures stabilized 7 kya. Our work will help us understand the sensitivity of the ice sheet to past climate changes, which is necessary to better predict its future stability.

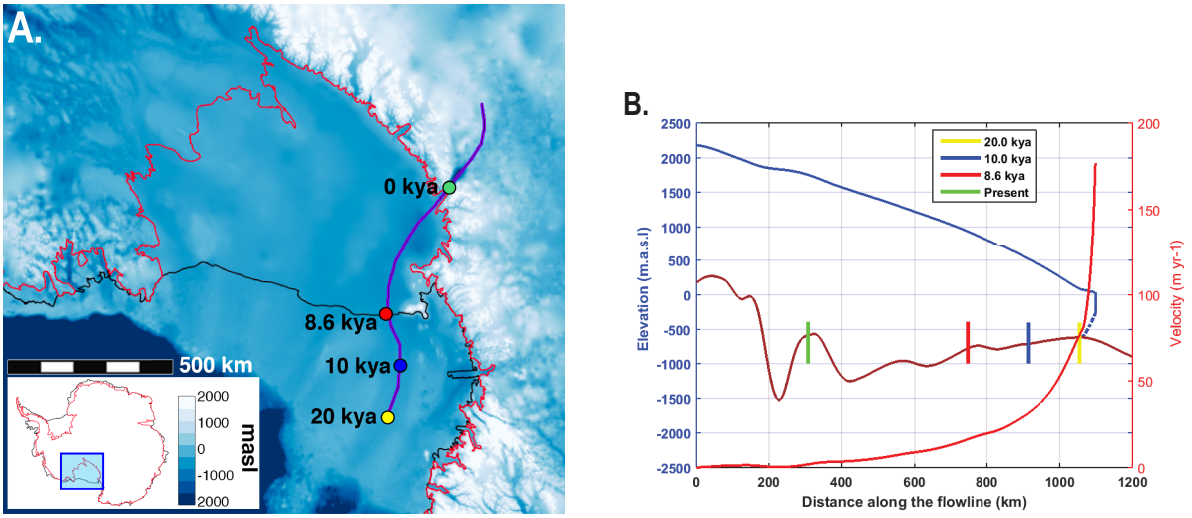

Figure 15: A). Byrd Glacier flowline used in this study, overlain on the BedMap2 DEM (Fretwell et al., 2013). The red line is the current grounding line from Rignot et al. (2011a), and the black line is the current ice shelf edge. Dated submarine moraines at 8.6 kya and 10 kya constrain ice shelf retreat. B). Steady state geometry and ice velocity of Byrd Glacier during the LGM. The four colored vertical lines represent the four colored subglacial moraines shown in panel A).

2.0 METHODS

Our model experiments investigate whether Byrd Glacier's pattern of retreat from its LGM position was controlled predominantly by atmospheric or oceanic perturbations.

2.1 Numerical model

In this study we use a one-dimensional, depth-integrated and width-averaged flowline model (Petrakopoulos et al., in preparation), similar to Nick et al. (2010). The model is based on conservation

of momentum and the depth-integrated continuity equation (van der Veen, 2013):

$$-AS\,[(H-\frac{\rho_w}{\rho_i}\ |H_{base}|)\ U]^{\frac{1}{3}}-2\frac{H}{W_{full}}\,(\frac{5U}{AW_{full}})^{\frac{1}{3}}+2\{\frac{\partial}{\partial x}[HA^{-\frac{1}{3}}\,|\frac{\partial U}{\partial x}|^{-\frac{2}{3}}\frac{\partial U}{\partial x}]\}\ =\ \rho_i\ g\ H\,(\frac{\partial HS}{\partial x}) \tag{9}$$

,

where g is the gravitational acceleration (9.806 m s^{-2}), ρ_w is the ocean water density (1025 kg m^{-3}) and ρ_i is the ice density (917 kg m^{-3}). H is the thickness of the glacier, x is the distance along the flowline, H_{base} is the bed elevation (negative below sea level), HS is the surface elevation, W_{full} is the glacier width, and U is the depth-integrated, width-averaged ice velocity.

The bed drag parameter AS is fixed, and the changes of the AS and the effective pressure expressed by the sliding parameter A_s. The exponent of the sliding relation, m is set to 3, following Nick et al. (2010). We use a rate factor A of 1.7 10^{-25} Pa^{-3} s^{-1} to 3.2 10^{-25} Pa^{-3} s^{-1} along our flowline, which is equivalent to an ice temperature of -18 °C to -11 °C, respectively (Cuffey & Paterson, 2010). We use the Weertman sliding relation to calculate basal drag (van der Veen, 1996), which assumes an easy connection between the subglacial drainage system and the open ocean. The model uses a small time step (0.0027 years), and the exponent of Glen's flow law, n, is set to 3. We solve the force balance equation (11), by calculating the depth-integrated glacier velocity (u); we calculate the ice thickness (H) from the next depth-integrated continuity equation (van der Veen, 2013):

$$\frac{\partial H}{\partial t}\ =\ -\ (\ \frac{1}{W_{full}}\ )\ \frac{\partial(H\ U\ W_{full})}{\partial x}+S\dot{M}B+M\dot{B}_{gl}+\dot{m}_{float}\ , \tag{10}$$

where $S\dot{M}B$ is the surface mass balance rate (snowfall, rain, sublimation and snowmelt), $M\dot{B}_{gl}$ is the mass balance rate at grounding line (due largely to submarine melt rates), and $\dot{m}_{float}$ is the submarine melt rate along the floating ice shelf. The atmospheric surface temperature increased during the LGM until the late Holocene period (Fleming et al., 1998; Petit et al., 1999; Jouzel et al., 2001; Peltier & Fairbanks, 2006; Parrenin et al., 2007). Despite the uncertainty in observations (e.g. Golledge et al., 2012; Whitehouse et al., 2012), we assume that warmer air is characterized by

increased moisture-carrying capacity. In this way, precipitation changes follow a temperature dependent function, as suggested by Huybrechts (2002) and Lenaerts et al. (2012). We calculate our temperature dependent function using surface temperatures from the ECBilt-CLIO paleoclimate modeling simulation (Timm & Timmermann, 2007) (Figure 16B). We constrain precipitation using SMB estimates from Pollard & DeConto (2009), which applies a 50% increase in precipitation values from the LGM to today. At the ice shelf edge, we use a calving criterion based on upper and lower bounds of ice thickness (after Bassis & Walker, 2012). The upper limit, 300 m, is the ice thickness at the shelf edge in steady state. The lower limit is 220 m, after Whitehouse et al. (2017). Each model experiment is run for 20,000 yrs.

2.2 Data input

Our numerical model requires bed and surface elevation data, as well as paleoclimate information. The initial ice sheet geometry and bathymetry, surface mass balance and submarine melt rates (-0.05 m yr^{-1}) are from Pollard & DeConto (2009), at 4 km resolution and smoothed by a linear least squares regression (Figure 15A). We create a steady state geometry of Byrd Glacier through a 100,000 year model spin up. Paleo-grounding line locations and dates are from ship-based bathymetry and sediment cores (Lauren Simkins, personal communication). The SMB is calculated each year by assuming a linear relationship between surface temperature and SMB (Schroeder, 1999). Temperature (and, therefore, SMB) increases from the LGM to 7 kya, after which time both parameters stabilized (Figure 16B). We apply an initial submarine melt rate of -0.05 m yr^{-1} (Pollard & DeConto, 2009). Throughout each 20,000 year experiment run, we modify the bed elevation according to results from the Pollard & DeConto (2009) model (Figure 16A), which takes into account regional sea level rise and glacial isostatic adjustments (GIA).

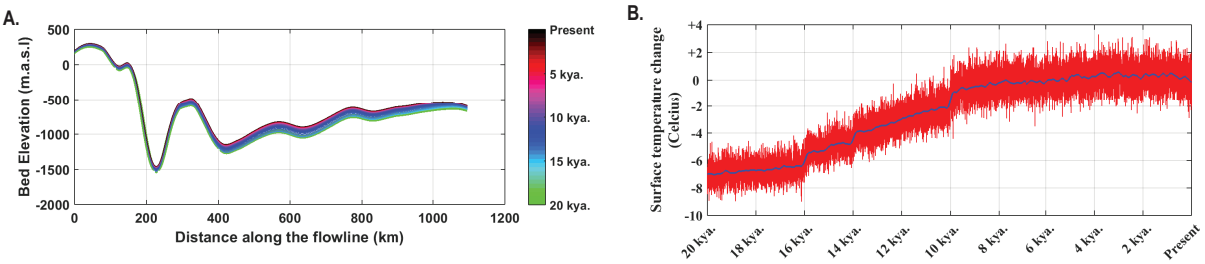

Figure 16: A) Bed topography along the Byrd Glacier flowline, as it adjusts from the LGM to present due to isostasy (Pollard & DeConto, 2009). B) Surface temperature change from the LGM to present (ECBilt-CLIO paleoclimate modeling simulation, Timm & Timmermann, 2007).

3.0 EXPERIMENTS

Following the Last Glacial Maximum (LGM), glaciers and ice streams that drained into the Ross Sea embayment retreated more than 250 km, creating an extended ice shelf (Anderson et al., 2002; Bentley et al., 2014). Throughout the retreat, some glaciers deposited subglacial features on the sea floor, the dates and locations of which can be used to constrain retreat in our model (Halberstadt et al., 2016). Our experiments are designed to investigate the environmental forcings that could have controlled the retreat of Byrd Glacier from its LGM configuration. In particular, we assess the relative importance of changes in surface mass balance near the grounding line and submarine melt beneath the ice shelf at different stages of retreat.

We use an inverse model where we adjust the environmental forcing (either mass balance at the grounding line or undercutting melting along the whole ice shelf) during each model time step so that the model matches the observed rate of retreat. We then assess whether the forcing variable was adjusted within reasonable limits. This technique is often used on larger scales where the basal sliding coefficient is adjusted to fit observed surface elevation or ice velocities (e.g. Brocq et al., 2009; Arthern & Gudmundsson, 2010; Jay-Allemand et al., 2011; Pralong & Gudmundsson, 2011; Pollard & DeConto, 2012).

For model simplicity, we constrain Byrd Glacier's retreat with four dated moraines along the flowline (Brecher, 1982; Hall et al., 2013; McKay et al., 2016), which we interpret as paleo-grounding line locations (Figure 17). In reality, there are several smaller moraines along the flowline as well

(Lauren Simkins, personal communication; Yokoyama et al., 2016). Our model runs begin 20 kya when Byrd Glacier was at its LGM position. Terrestrial glacial geological data suggest that grounding line retreat began 13 kya (Hall et al., 2013) and radiocarbon dated sediment cores show that the grounding line was near the current ice shelf edge at 8.6 kya (McKay et al., 2016). We use a linear approximation for retreat rates between the dated points at 20 kya, 13 kya and 8.6 kya, but because there are no dated features under the present (752 km long) Ross Ice Shelf, we test three different retreat patterns for this region. In the first scenario, we force a linear retreat of the grounding line from 8.6 kya to present. In the second scenario, we assume that the grounding line underwent a non-linear and rapid retreat to its current configuration, starting 3 kya. In the third scenario, the grounding line retreats rapidly so that it reaches its current configuration by 4 kya.

3.1 Experiment ♯1: Oceanic forcing along ice shelf

Several modeling studies suggest that ocean warming caused the retreat of the East Antarctic Ice Sheet after the LGM (Mackintosh et al., 2011; Golledge et al., 2012; Mackintosh et al., 2014). However, our knowledge of ocean temperatures and circulation patterns over the past 20 kyr is limited to paleoclimate models, which have large uncertainties.

In our experiments, we force the model to match the observed retreat patterns by adjusting submarine melt rates along the whole ice shelf at each time step (Figure 17). When the glacier is in steady state (at the LGM position), we set the melt rate to -0.1 m yr^{-1} (after Pollard & DeConto, 2009), 1 km from the grounding line position, decreasing linearly to zero at the grounding line.

Our model results are forced to mimic the observed grounding line evolution, but all runs failed to create the present geometry (mainly, surface elevation) of Byrd Glacier (Figure 17A, C, E). Furthermore, in order to model the observed rate of retreat, extremely high values of submarine melt rate (100 times the initial rate of -10 m yr^{-1}) are needed for all scenarios between 12 kya and 8 kya, and for the first and second scenarios in the last 2 kyr (Figure 17B, D). For the third scenario, where the grounding line is forced to rapidly retreat between 8.6 kya and 4 kya when it reaches its present configuration, submarine melt must be -70 m yr^{-1}, which is likely unreasonable.

In addition, a floating ice shelf cannot exist with these high submarine melt rates.

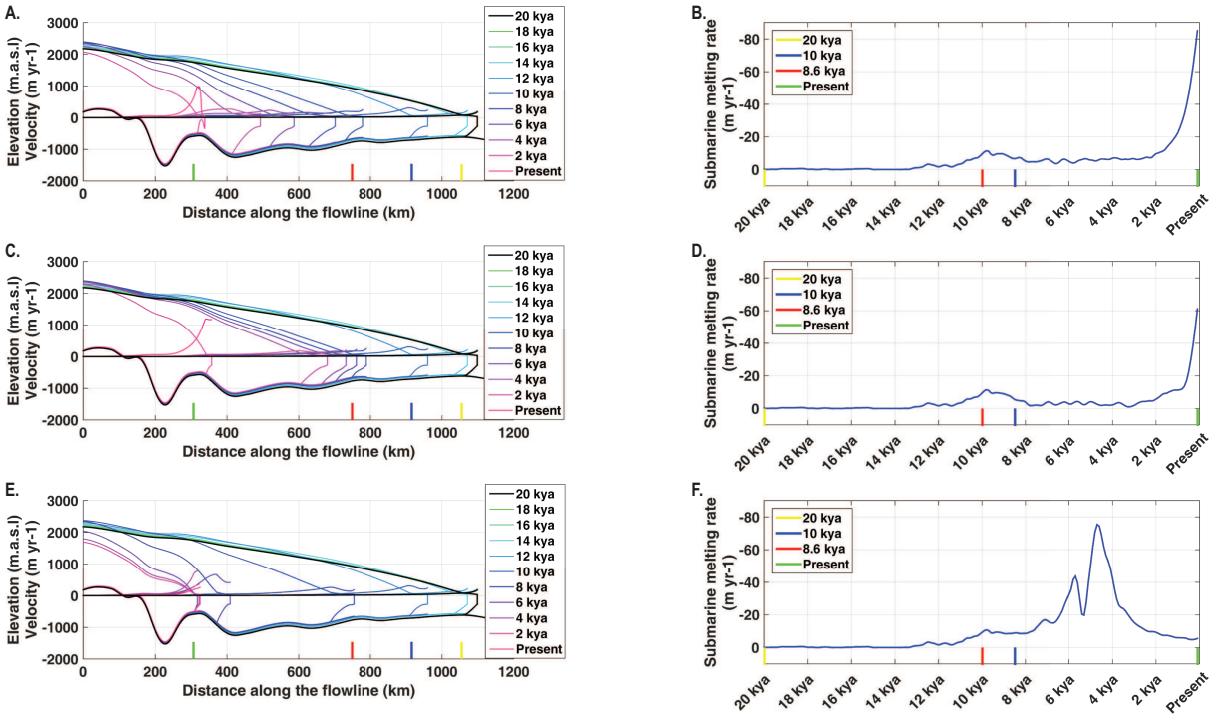

Figure 17: Glacier geometry and ice velocity profiles under the first (A), second (C) and third (E) submarine melt retreat scenarios. Profiles are drawn every 2 kyr. The recorded temporal evolution for the maximum submarine melt rate, 1 km front of grounding line, for the first (B), second (D) and third (F) retreat scenarios.

3.2 Experiment ♯2: Environmental forcings near and at grounding line

3.2.1 Negative Mass balance at grounding line

We assess whether temporal variations in mass balance (MB) near the grounding line can reproduce Byrd Glacier's evolution. As before, we force the model to follow one of the proposed rates of retreat. Based on mass flux estimates of 23 Antarctic glaciers and ice shelves, the basal melt rate at the Byrd Glacier grounding line is estimated to be -15 m yr^{-1} (Rignot & Jacobs, 2002). According to their results, basal melt rates are directly correlated with increased ocean temperatures, although they could also be related to intermittent subglacial floods (Stearns et al., 2008; Jenkins, 2011), or the presence of Blue Ice Areas near the grounding line (Ligtenberg et al., 2014). Subglacial

flooding events have the potential to cause rapid and intermittent high melt due to the upwelling of freshwater water at the grounding line. Blue Ice Areas (BIAs) extend over the current trunk and grounding line of Byrd Glacier and are estimated to have negative SMB values of -0.35 m yr^{-1} (Lenaerts et al., 2012; Ligtenberg et al., 2014). The formation of BIAs can be self–sustaining because sublimation rates increase with the lower albedo of the blue ice (Bintanja & Broeke, 1995) and the smooth texture of blue ice does not permit snow accumulate on the surface (van den Broeke & Bintanja, 1995). We are unable to differentiate between the source of the mass balance change at the grounding line in this study; instead, we focus on the impact that this change has on the retreat rate.

We perturb the steady state Byrd Glacier profile by applying a negative mass balance rate at the grounding line. We use an average rate of 1 m yr^{-1}, with a minimum of 2 m yr^{-1}. Negative MB near the grounding line forces the glacier to thin, and subsequently retreat. From the three retreat patterns, the third requires likely unrealistically negative values of MB between 8 kya and 2 kya (Figure 18F), and is therefore not a plausible scenario. We consider as the most plausible scenario the second scenario, where the final geometry consists of a long ice shelf (Figure 18C) and requires the smallest values of mass balance change (Figure 18D) of all scenarios.

3.2.2. Decreasing basal friction near grounding line

In this section we test whether we can achieve the observed retreat patterns by adjusting only the sliding parameter, A_s. First, we introduce an instantaneous perturbation where we reduce the basal drag by 20% at 10 km up-flow of the grounding line, and 50% at 40 km up-flow of the grounding line. We apply the perturbation at 13 kya, and the results show that Byrd Glacier either does not retreat or undergoes a small advance as mass is advected down-flow. Second, we conduct an inverse model of the retreat pattern, where we continuously modify the sliding parameter A_s in the last 20 km from the grounding line. We find that the glacier can only mimic the observed retreat patterns if the sliding parameter, A_s, increases to a likely unrealistic value.

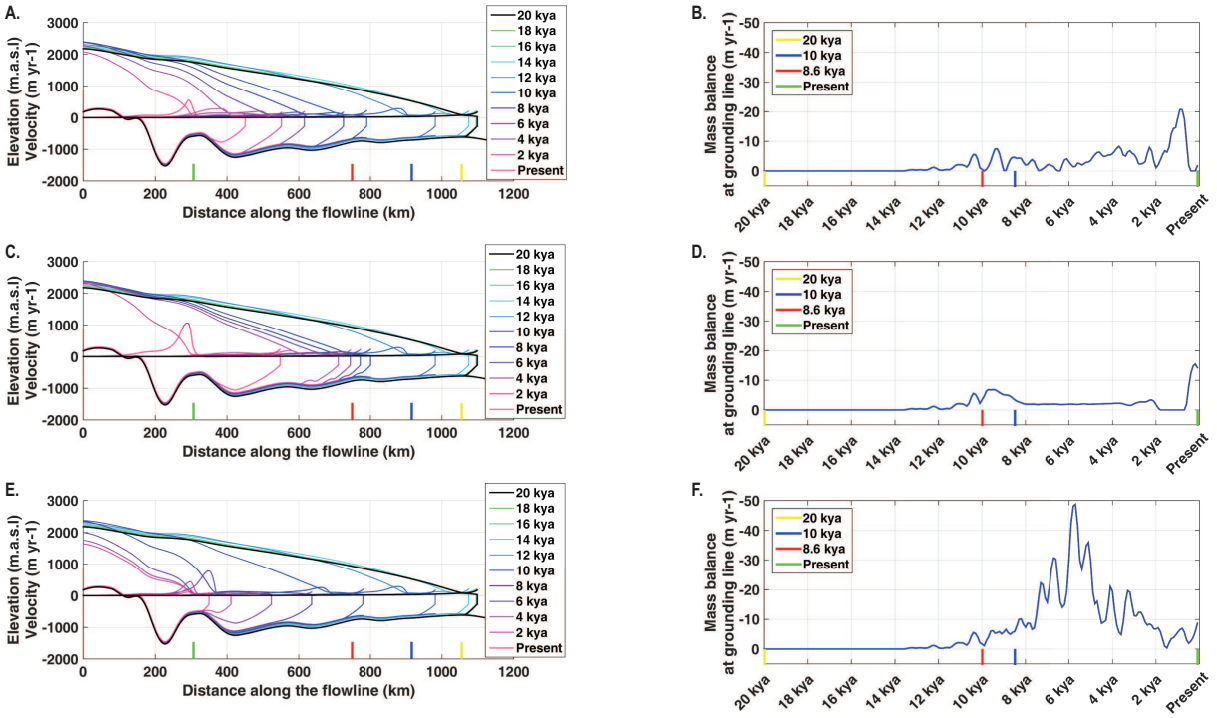

Figure 18: Glacier geometry and ice velocity profiles in the first (A), second (C) and third (E) retreat scenarios, if only mass balance at the grounding line is adjusted. Profiles are drawn every 2 kyr. In order to simulate the observed retreat, the mass balance needs to be adjusted for the first (B), second (D) and third (F) retreat scenarios.

3.3 Experiment ♯3: Combined forcing

Ocean melting along the ice shelf and changes in mass balance at the grounding line likely occur in tandem, so we conduct two final experiments to assess how the retreat may have varied under a combined perturbation for scenario ♯2. From 20 kya to 4 kya, we reduce the mass balance at the grounding line of Byrd Glacier; from 4 kya to present we increase submarine melting beneath the ice shelf (from -0.1 m yr^{-1} to -0.5 m yr^{-1}). In both experiments, we force the model to follow retreat scenario ♯2 by adjusting the MB near the grounding line.

Adding ocean melting to the MB change at the grounding line leads to a smaller, and likely more realistic, change in MB at the grounding line during the last 4 kya (Figure 19B). This experiment also creates a longer ice shelf (Figure 19A) than in experiment ♯2 (Figure 18D), but does not manage to create an ice shelf as long as the current Ross Ice Shelf.

In the second experiment, in order to create an ice shelf that extends the full length of the current

Ross Ice Shelf (red circle at 752 km, Figure 15), we adjust the terminus thickness to reach our lower limit of 220 m. An ice shelf forms that is similar to the present day Ross Ice Shelf (Figure 19C), and the velocity near the grounding line is comparable to the current velocity (Stearns et al., 2008). The desired retreat is modeled for the last 4 kya, with a smaller (and likely more realistic) change in MB at the grounding line than in any other experiment (Figure 19D).

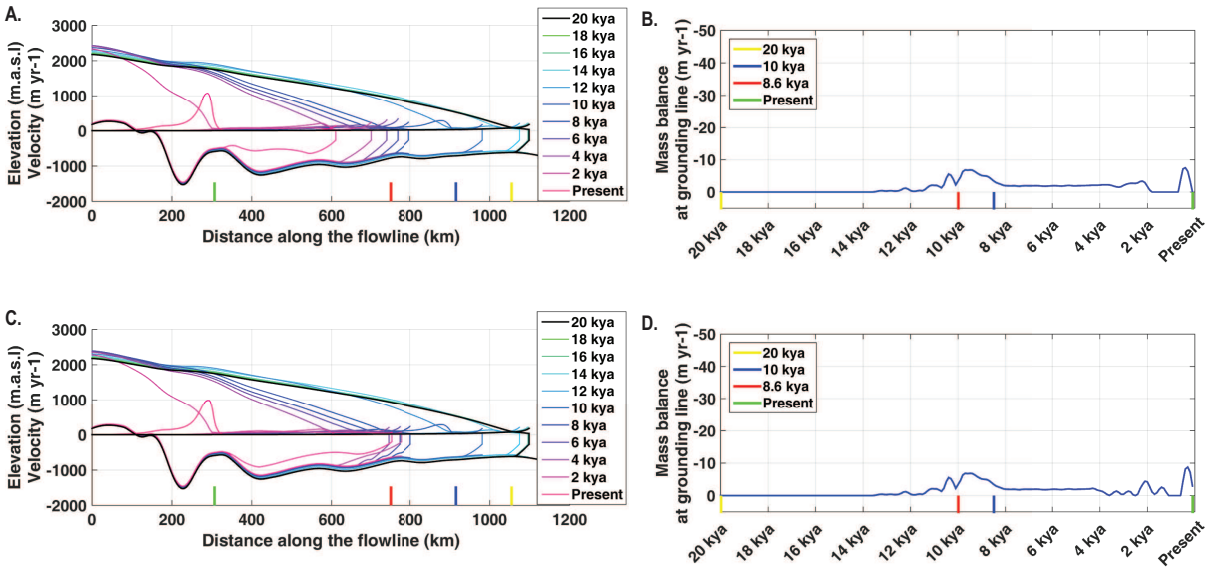

Figure 19: A) Glacier geometry and ice velocity profiles under retreat scenario ♯2 for the combined forcing perturbation. Profiles are drawn every 2 kyr. The last 4 kyr we increase and change the maximum submarine melting rate from -0.1 m yr^{-1}, 1km away from grounding line, to -0.5 m yr^{-1}, 10 km away respectively. B) The MB at the grounding line that is needed to achieve the observed retreat pattern in panel A). C) Profiles from the identical experiment as in panel A), but with a 35% (135m to 100m) decrease in crevasse water depth. D) The MB at the grounding line that is needed to achieve the observed retreat pattern in panel C).

4.0 DISCUSSION

Our modeling results show that decreases in mass balance at the grounding line of Byrd Glacier are needed in order to simulate the observed rate of retreat while also preserving a long ice shelf. Scenario ♯2 appears to be the most plausible of our tested scenarios because it is the only one that can match the retreat patterns and the current geometry and velocity of Byrd Glacier while sustaining a long ice shelf. Scenario ♯2 assumes rapid and non-linear retreat from 3 kya to present

day, requiring large adjustments in mass balance at the grounding line at 3 kya and between 11 and 8.6 kya (Figure 19D). These mass balance adjustment can come from enhanced surface mass loss (growth of Blue Ice Areas), or increases in submarine melting either from warmer ocean temperatures or turbulent plumes due to periodic subglacial lake drainage events. Regardless of the mechanism, grounding line mass loss needs to increase from 0.1 m yr^{-1} to a maximum 2 m yr^{-1} in order to simulate Byrd Glacier's retreat.

While we cannot isolate the particular mechanism, mass balance adjustments at the grounding line of Byrd Glacier drive its retreat. One hypothesis is that the formation of BIAs enhance mass loss. Mass balance might be expected to become more negative as Byrd Glacier retreats, causing surface slopes to be steeper, increasing the strength of katabatic winds that help form BIAs. Furthermore, the increased surface temperature (Figure 16B) creates the conditions for enhanced snow erosion, surface melting, drifting snow, and sublimation near the grounding line, a mechanism that is described in detail by Lenaerts et al. (2017); sublimation rates for Byrd Glacier are estimated to be -0.35 m yr^{-1} (Lenaerts et al., 2012; Ligtenberg et al., 2014). A second hypothesis is that ocean warming caused an increase in submarine melting at the grounding line (Rignot & Jacobs, 2002). As Byrd Glacier's grounding line retreated into deeper water, a positive feedback mechanism could have progressively increased melting by continuously transferring ocean heat at the grounding line, through an incursion of Circumpolar Deep Water (CDW) onto the shelf (Golledge et al., 2014). A third hypothesis is that enhanced submarine melting at the grounding line is caused by periodic draining of subglacial floods which form turbulent plumes that can erode ice at the grounding line (e.g. Stearns et al., 2008).

Sediment cores, terrestrial glacial geological data and glaciological evidence show that glaciers in the Ross Sea embayment, including Byrd Glacier, remained at their LGM position from 20 kya until 13 kya (Hall et al., 2013). Furthermore, the Ross Ice Shelf edge has been near Ross Island since ~8.9 kya, while the grounding line retreated towards its current location (McKay et al., 2016). Scenario ♯2 mimics this chronology – the ice shelf edge remains at this position from ~8 kya to present day while the grounding line continuously retreated (Figure 19B). Persistent grounding

line retreat led to the formation of the long Ross Ice Shelf approximately 4 kya (Figure 19B). Negative mass balance at the grounding line is crucial in driving grounding line retreat, especially from 3 – 1 kya when retreat was rapid. Not surprisingly, we show that processes controlling mass balance at the grounding line control the length of the ice shelf (location of the grounding line), while submarine melting along the ice shelf controls its thickness.

There is a debate as to whether environmental forcings, including submarine melting and mass balance adjustments tested here, or topography modulate glacier retreat. Our model results suggest that, at different epochs, there is a different control on retreat. For example, in our final experiment (Section 3.3), melt at the grounding line and along the ice shelf are needed to create an ice shelf that is similar in geometry as the Ross Ice Shelf. However, our results also show that the Byrd Glacier grounding line would continue to retreat between 7 kya and present, even if the forcing stayed the same (Figure 16B). Similarly, from 2 kya to present, the Byrd Glacier grounding line retreated through a very deep bed trough (>1000 m) in the Ross Sea. Observational and theoretical studies suggest that glaciers are unstable on reverse slopes, causing acceleration and rapid retreat until the grounding line can stabilize on a submarine high (e.g. Nick et al., 2007). Scenario ♯2 adopts this behavior, and the mass balance results show that the glacier continues to retreat without being forced by any mechanism (Figure 18D).

Several studies suggest that retreat of the Antarctic Ice Sheet from its Last Glacial Maximum position was due to a combination of changes in ocean heat, atmospheric warming, and eustatic sea level from melting of Northern Hemisphere ice sheets (Pollard & DeConto, 2009; Mackintosh et al., 2011; Davies et al., 2014). However, glacier basins respond to environmental forcings based on their individual dynamics, namely whether their ice velocity is dominated by viscous creep or basal sliding (Golledge et al., 2012). For example, a glacier dominated by viscous creep will likely respond slowly to ocean forcings, even if the forcing is large. On Byrd Glacier, where basal sliding at the grounding line is relatively large, ocean forcings imposed at the grounding line have a fairly rapid effect on glacier retreat as well as thinning rates and ice velocity. If submarine melting is applied to the whole floating ice shelf, as opposed to focused at the grounding line, then there

is minimal and delayed retreat of the grounding line. Further, our modeled evolution of Byrd Glacier differs from that found in Pollard & DeConto (2009). In Pollard & DeConto (2009) model [Paleoclimate Modelling Intercomparison Project (PMIP)], the retreat of Byrd Glacier does not fit with the paleo-grounding line measurements. They also suggest that the Ross Ice Shelf formed very quickly between 16 kya and 15 kya. In our results the Ross Ice Shelf forms more slowly at 4 kya.

Our research indicates the complexity of Byrd Glacier's behavior to variations in mass balance at grounding line, as well as in fluctuations in the submarine melt rate. The knowledge of the bed geometry underneath the ice shelf, and the detailed chronological evolution of Byrd's grounding line since LGM, will provide us with crucial information about the temporal and spatial evolution of both mechanisms. Additional information on the bed topography near the grounding line is important to increasing our model validity.

5.0 CONCLUSIONS

We use an one dimensional flowline model to investigate the retreat of Byrd Glacier since the Last Glacial Maximum (LGM). In particular, we examine whether the retreat was the output of mass balance fluctuations at the grounding line or along the ice shelf. We show that both mechanisms are important for Byrd Glacier's retreat, but the negative mass valance at the grounding line plays a dominant role, particularly in the last 4-6 kya. Our modeling results suggest that the Ross Ice Shelf likely formed ~4 kya.

CONCLUSIONS

In this dissertation, we incorporate observational and modeled data into a new numerical prognostic flowline model aimed at increasing our current ability to predict the behavior of glacier flow and their contribution to sea level rise. We simulate and evaluate the behavior of real glaciers, such as Helheim Glacier in Southwest Greenland and Byrd Glacier in East Antarctica, in different climate scenarios. We also test the sensitivity of glaciers to atmospheric and oceanic perturbations, and the role of the geometry in glacier behavior.

For Greenland tidewater glaciers, we show that both atmospheric and oceanic forcings can influence the glacier behavior in decadal time scale. However, changes associated with the ice-bed interface result in larger and more long-lived changes to ice discharge than changes at the ice-ocean interface. Furthermore, we show that modifications in bed and width profiles play a small role in varying the mass loss of retreating glaciers. Glaciers with narrow sections far from the terminus have the largest impact on reducing in glacier discharge. Finally, in the last chapter, we show that both atmospheric and oceanic forcings played a role during the retreat of Byrd Glacier since the LGM. Byrd Glacier was continue to respond after temperatures have stabilized 7,000 years ago, reaching to the current configuration 1,000 to 2,000 years ago. The last 3,000 years, the role of the negative mass balance at grounding line was crucial for the formation of the present long ice shelf.

References

Amundson, J. M. & Truffer, M. (2010). A unifying framework for iceberg-calving models. *Journal of Glaciology*, 56(199), 822–830.

Amundson, J. M., Truffer, M., Lüthi, M. P., Fahnestock, M., West, M., & Motyka, R. J. (2008). Glacier, fjord, and seismic response to recent large calving events, Jakobshavn Isbræ, Greenland. *Geophysical Research Letters*, 35(22). L22501.

Andersen, M. L., Larsen, T. B., Nettles, M., Elosegui, P., van As, D., Hamilton, G. S., Stearns, L. A., Davis, J. L., Ahlstrøm, A. P., de Juan, J., Ekström, G., Stenseng, L., Khan, S. A., Forsberg, R., & Dahl-Jensen, D. (2010). Spatial and temporal melt variability at Helheim Glacier, East Greenland, and its effect on ice dynamics. *Journal of Geophysical Research: Earth Surface*, 115(F4). F04041.

Anderson, J. B., Conway, H., Bart, P. J., Witus, A. E., Greenwood, S. L., McKay, R. M., Hall, B. L., Ackert, R. P., Licht, K., Jakobsson, M., & Stone, J. O. (2014). Ross Sea paleo-ice sheet drainage and deglacial history during and since the {LGM}. *Quaternary Science Reviews*, 100, 31 – 54.

Anderson, J. B., Shipp, S. S., Lowe, L. A., Wellner, S. J., & Mosola, B. A. (2002). The Antarctic Ice Sheet during the Last Glacial Maximum and its subsequent retreat history: a review. *Quaternary Science Reviews*, 21(1–3), 49 – 70.

Anderson, R. F., Ali, S., Bradtmiller, L. I., Nielsen, S. H. H., Fleisher, M. Q., Anderson, B. E., &

Burckle, L. H. (2009). Wind-Driven Upwelling in the Southern Ocean and the Deglacial Rise in Atmospheric CO2. *Science*, 323(5920), 1443–1448.

Arthern, R. J. & Gudmundsson, G. H. (2010). Initialization of ice-sheet forecasts viewed as an inverse Robin problem. *Journal of Glaciology*, 56(197), 527–533.

Barrows, T. T., Juggins, S., De Deckker, P., Calvo, E., & Pelejero, C. (2007). Long-term sea surface temperature and climate change in the Australian–New Zealand region. *Paleoceanography*, 22(2).

Bartholomaus, T. C., Stearns, L. A., Sutherland, D. A., Shroyer, E. L., Nash, J. D., Walker, R. T., Catania, G., Felikson, D., Carroll, D., Fried, M. J., & others. (2016). Contrasts in the response of adjacent fjords and glaciers to ice-sheet surface melt in West Greenland. *Annals of Glaciology*, 57(73), 25–38.

Bassis, J. & Walker, C. (2012). Upper and lower limits on the stability of calving glaciers from the yield strength envelope of ice. *Proceedings of the Royal Society A: Mathematical, Physical and Engineering Sciences*, 468(2140), 913–931.

Benn, D. I., Warren, C. R., & Mottram, R. H. (2007). Calving processes and the dynamics of calving glaciers. *Earth-Science Reviews*, 82(3–4), 143 – 179.

Bentley, M. J., Cofaigh, C. ., Anderson, J. B., Conway, H., Davies, B., Graham, A. G., Hillenbrand, C.-D., Hodgson, D. A., Jamieson, S. S., Larter, R. D., Mackintosh, A., Smith, J. A., Verleyen, E., Ackert, R. P., Bart, P. J., Berg, S., Brunstein, D., Canals, M., Colhoun, E. A., Crosta, X., Dickens, W. A., Domack, E., Dowdeswell, J. A., Dunbar, R., Ehrmann, W., Evans, J., Favier, V., Fink, D., Fogwill, C. J., Glasser, N. F., Gohl, K., Golledge, N. R., Goodwin, I., Gore, D. B., Greenwood, S. L., H., B. L., Hall, K., Hedding, D. W., Hein, A. S., Hocking, E. P., Jakobsson, M., Johnson, J. S., Jomelli, V., Jones, R. S., Klages, J. P., Kristoffersen, Y., Kuhn, G., Leventer, A., Licht, K., Lilly, K., Lindow, J., Livingstone, S. J., Massé, G., McGlone, M. S., McKay, R. M., Melles, M., Miura, H., Mulvaney, R., Nel, W., Nitsche, F. O., O'Brien, P. E., Post, A. L., Roberts, S. J.,

Saunders, K. M., Selkirk, P. M., Simms, A. R., Spiegel, C., Stolldorf, T. D., Sugden, D. E., van der Putten, N., van Ommen, T., Verfaillie, D., Vyverman, W., Wagner, B., White, D. A., Witus, A. E., & Zwartz, D. (2014). A community-based geological reconstruction of Antarctic Ice Sheet deglaciation since the Last Glacial Maximum. *Quaternary Science Reviews*, 100, 1 – 9.

Bevan, S. L., Luckman, A., Khan, A. A., & Murray, T. (2015). Seasonal dynamic thinning at Helheim Glacier. *Earth and Planetary Science Letters*, 415, 47 – 53.

Bevan, S. L., Luckman, A. J., & Murray, T. (2012). Glacier dynamics over the last quarter of a century at Helheim, Kangerdlugssuaq and 14 other major Greenland outlet glaciers. *The Cryosphere*, 6(5), 923–937.

Bindoff, N. L., Willebrand, J., Artale, V., Cazenave, A., Gregory, J. M., Gulev, S., Hanawa, K., Le Quéré, C., Levitus, S., Nojiri, Y., et al. (2007). Observations: oceanic climate change and sea level.

Bintanja, R. & Broeke, M. R. V. D. (1995). The Surface Energy Balance of Antarctic Snow and Blue Ice. *Journal of Applied Meteorology*, 34(4), 902–926.

Brecher, H. H. (1982). Photogrammetric Investigation of Byrd Glacier Surface Lowering (Abstract only). *Annals of Glaciology*, 3, 353–353.

Brocq, A. L., Payne, A., Siegert, M., & Alley, R. (2009). A subglacial water-flow model for West Antarctica. *Journal of Glaciology*, 55(193), 879–888.

Carr, J., Vieli, A., Stokes, C., Jamieson, S., Palmer, S., Christoffersen, P., Dowdeswell, J., Nick, F., Blankenship, D., & Young, D. (2015). Basal topographic controls on rapid retreat of Humboldt Glacier, northern Greenland. *Journal of glaciology.*, 61(225), 137–150.

Carr, J. R., Vieli, A., Stokes, C. R., Jamieson, S. S. R., Palmer, S. J., Christoffersen, P., Dowdeswell, J. A., Nick, F. M., Blankenship, D. D., & Young, D. A. (2015). Basal topographic

controls on rapid retreat of Humboldt Glacier, northern Greenland. *Journal of Glaciology*, 61, 137–150.

Carroll, D., Sutherland, D. A., Shroyer, E. L., Nash, J. D., Catania, G. A., & Stearns, L. A. (2015). Modeling Turbulent Subglacial Meltwater Plumes: Implications for Fjord-Scale Buoyancy-Driven Circulation. *Journal of Physical Oceanography*, 45(8), 2169–2185.

Christoffersen, P., Mugford, R. I., Heywood, K. J., Joughin, I., Dowdeswell, J. A., Syvitski, J. P. M., Luckman, A., & Benham, T. J. (2011). Warming of waters in an East Greenland fjord prior to glacier retreat: mechanisms and connection to large-scale atmospheric conditions. *The Cryosphere*, 5(3), 701–714.

Christoffersen, P., O'Leary, M., Van Angelen, J. H., & Van Den Broeke, M. (2012). Partitioning effects from ocean and atmosphere on the calving stability of Kangerdlugssuaq Glacier, East Greenland. *Annals of Glaciology*, 53, 249–256.

Clark, P. U., Dyke, A. S., Shakun, J. D., Carlson, A. E., Clark, J., Wohlfarth, B., Mitrovica, J. X., Hostetler, S. W., & McCabe, A. M. (2009). The Last Glacial Maximum. *Science*, 325(5941), 710–714.

Cook, S., Rutt, I. C., Murray, T., Luckman, A., Zwinger, T., Selmes, N., Goldsack, A., & James, T. D. (2014). Modelling environmental influences on calving at Helheim Glacier in eastern Greenland. *The Cryosphere*, 8(3), 827–841.

Csatho, B. M., Schenk, A. F., van der Veen, C. J., Babonis, G., Duncan, K., Rezvanbehbahani, S., van den Broeke, M. R., Simonsen, S. B., Nagarajan, S., & van Angelen, J. H. (2014). Laser altimetry reveals complex pattern of Greenland Ice Sheet dynamics. *Proceedings of the National Academy of Sciences*, 111(52), 18478–18483.

Cuffey, K. & Paterson, W. S. B. (2010). *The physics of glaciers*. Burlington, MA Elsevier, 4th edition.

Davies, B. J., Golledge, N. R., Glasser, N. F., Carrivick, J. L., Ligtenberg, S. R. M., Barrand, N. E., van den Broeke, M. R., Hambrey, M. J., & Smellie, J. L. (2014). Modelled glacier response to centennial temperature and precipitation trends on the Antarctic Peninsula. *Nature*, 4(11), 993–998.

Davis, J. L., de Juan Verger, J., Elosegui, P., Nettles, M., & Andersen, M. L. (2013). Evidence for Non-tidal Diurnal Velocity Variations of Helheim Glacier, East Greenland. *AGU Fall Meeting Abstracts*.

Denton, G. H. & Hughes, T. J. (2002). Reconstructing the Antarctic Ice Sheet at the Last Glacial Maximum. *Quaternary Science Reviews*, 21(1–3), 193 – 202.

Durkin, W. J., Bartholomaus, T. C., Willis, M. J., & Pritchard, M. E. (2017). Dynamic Changes at Yahtse Glacier, the Most Rapidly Advancing Tidewater Glacier in Alaska. *Frontiers in Earth Science*, 5, 21.

Enderlin, E. M., Howat, I. M., & Vieli, A. (2012). High Sensitivity of Tidewater Glacier Dynamics to Shape. *AGU Fall Meeting Abstracts*.

Enderlin, E. M., Howat, I. M., & Vieli, A. (2013). The sensitivity of flowline models of tidewater glaciers to parameter uncertainty. *The Cryosphere*, 7(5), 1579–1590.

Fleming, K., Johnston, P., Zwartz, D., Yokoyama, Y., Lambeck, K., & Chappell, J. (1998). Refining the eustatic sea-level curve since the Last Glacial Maximum using far- and intermediate-field sites. *Earth and Planetary Science Letters*, 163(1–4), 327 – 342.

Foga, S., Stearns, L. A., & van der Veen, C. J. (2014). Application of Satellite Remote Sensing Techniques to Quantify Terminus and Ice Melange Behavior at Helheim Glacier, East Greenland. *Marine Technology Society Journal*, 48(5), 81–91.

Fretwell, P., Pritchard, H. D., Vaughan, D. G., Bamber, J. L., Barrand, N. E., Bell, R., Bianchi, C., Bingham, R. G., Blankenship, D. D., Casassa, G., Catania, G., Callens, D., Conway, H.,

Cook, A. J., Corr, H. F. J., Damaske, D., Damm, V., Ferraccioli, F., Forsberg, R., Fujita, S., Gim, Y., Gogineni, P., Griggs, J. A., Hindmarsh, R. C. A., Holmlund, P., Holt, J. W., Jacobel, R. W., Jenkins, A., Jokat, W., Jordan, T., King, E. C., Kohler, J., Krabill, W., Riger-Kusk, M., Langley, K. A., Leitchenkov, G., Leuschen, C., Luyendyk, B. P., Matsuoka, K., Mouginot, J., Nitsche, F. O., Nogi, Y., Nost, O. A., Popov, S. V., Rignot, E., Rippin, D. M., Rivera, A., Roberts, J., Ross, N., Siegert, M. J., Smith, A. M., Steinhage, D., Studinger, M., Sun, B., Tinto, B. K., Welch, B. C., Wilson, D., Young, D. A., Xiangbin, C., & Zirizzotti, A. (2013). Bedmap2: improved ice bed, surface and thickness datasets for Antarctica. *The Cryosphere*, 7(1), 375–393.

Gleick, P. H. (1993). *Water in crisis: a guide to the worlds fresh water resources.* New York New York Oxford University Press 1993.

Golledge, N. R., Fogwill, C. J., Mackintosh, A. N., & Buckley, K. M. (2012). Dynamics of the last glacial maximum Antarctic ice-sheet and its response to ocean forcing. *Proceedings of the National Academy of Sciences*, 109(40), 16052–16056.

Golledge, N. R., Menviel, L., Carter, L., Fogwill, C. J., England, M. H., Cortese, G., & Levy, R. H. (2014). Antarctic contribution to meltwater pulse 1A from reduced Southern Ocean overturning. *Nature Communications*, 5, 5107.

Gudmundsson, G. H., Krug, J., Durand, G., Favier, L., & Gagliardini, O. (2012). The stability of grounding lines on retrograde slopes. *The Cryosphere*, 6, 1497– 1505.

Halberstadt, A. R. W., Simkins, L. M., Greenwood, S. L., & Anderson, J. B. (2016). Past ice-sheet behaviour: retreat scenarios and changing controls in the Ross Sea, Antarctica. *The Cryosphere*, 10(3), 1003–1020.

Hall, B. L., Denton, G. H., Stone, J. O., & Conway, H. (2013). History of the grounded ice sheet in the Ross Sea sector of Antarctica during the Last Glacial Maximum and the last termination. *Geological Society, London, Special Publications*, 381(1), 167–181.

Howat, I. (2016). MEaSURES Greenland Ice Velocity: Selected Glacier Site Velocity Maps from Optical Images, Version 1. Boulder, CO, USA. NASA National Snow and Ice Data Center Distributed Active Archive Center,. *(https://doi.org/10.5067/EYV1IP7MUNSV)*.

Howat, I. M., Box, J. E., Ahn, Y., Herrington, A., & McFadden, E. M. (2010). Seasonal variability in the dynamics of marine-terminating outlet glaciers in Greenland. *Journal of Glaciology*, 56, 601–613.

Howat, I. M., Joughin, I., Fahnestock, M., Smith, B. E., & Scambos, T. A. (2008). Synchronous retreat and acceleration of southeast Greenland outlet glaciers 2000-06: ice dynamics and coupling to climate. *Journal of Glaciology*, 54(187), 646–660.

Howat, I. M., Joughin, I., & Scambos, T. A. (2007). Rapid Changes in Ice Discharge from Greenland Outlet Glaciers. *Science*, 315(5818), 1559–1561.

Howat, I. M., Joughin, I., Tulaczyk, S., & Gogineni, S. (2005). Rapid retreat and acceleration of Helheim Glacier, east Greenland. *Geophysical Research Letters*, 32(22).

Howat, I. M., Negrete, A., & Smith, B. E. (2014). The Greenland Ice Mapping Project (GIMP) land classification and surface elevation data sets. *The Cryosphere*, 8(4), 1509–1518.

Hughes, T. J. (1981). The weak underbelly of the West Antarctic ice sheet. *Journal of Glaciology*, 27, 518–525.

Huybrechts, P. (2002). Sea-level changes at the {LGM} from ice-dynamic reconstructions of the Greenland and Antarctic ice sheets during the glacial cycles. *Quaternary Science Reviews*, 21(1–3), 203 – 231.

Iken, A. & Bindschadler, R. A. (1986). Combined measurements of Subglacial Water Pressure and Surface Velocity of Findelengletscher, Switzerland: Conclusions about Drainage System and Sliding Mechanism. *Journal of Glaciology*, 32(110), 101–119.

Jamieson, S. S. R., Vieli, A., Livingstone, S. J., Cofaigh, C. O., Stokes, C., Hillenbrand, C., & Dowdeswell, J. A. (2012). Ice-stream stability on a reverse bed slope. *Nature*, 5(11), 799–802.

Jay-Allemand, M., Gillet-Chaulet, F., Gagliardini, O., & Nodet, M. (2011). Investigating changes in basal conditions of Variegated Glacier prior to and during its 1982-1983 surge. *The Cryosphere*, 5(3), 659–672.

Jenkins, A. (2011). Convection-Driven Melting near the Grounding Lines of Ice Shelves and Tidewater Glaciers. *Journal of Physical Oceanography*, 41(12), 2279–2294.

Jensen, T. S., Box, J. E., & Hvidberg, C. S. (2016). A sensitivity study of annual area change for Greenland ice sheet marine terminating outlet glaciers: 1999–2013. *Journal of Glaciology*, 62(231), 72–81.

Joughin, I., Howat, I., Alley, R. B., Ekstrom, G., Fahnestock, M., Moon, T., Nettles, M., Truffer, M., & Tsai, V. C. (2008). Ice-front variation and tidewater behavior on Helheim and Kangerdlugssuaq Glaciers, Greenland. *Journal of Geophysical Research: Earth Surface*, 113(F1). F01004.

Joughin, I., Smith, B. E., & Abdalati, W. (2010a). Glaciological advances made with interferometric synthetic aperture radar. *Journal of Glaciology*, 56, 1026–1042.

Joughin, I., Smith, B. E., Howat, I. M., Scambos, T., & Moon, T. (2010b). Greenland flow variability from ice-sheet-wide velocity mapping. *Journal of Glaciology*, 56, 415–430.

Jouzel, J., Masson, V., Cattani, O., Falourd, S., Stievenard, M., Stenni, B., Longinelli, A., Johnsen, S. J., Steffenssen, J. P., Petit, J. R., Schwander, J., Souchez, R., & Barkov, N. I. (2001). A new 27 ky high resolution East Antarctic climate record. *Geophysical Research Letters*, 28(16), 3199–3202.

Kamb, B. (1987). Glacier surge mechanism based on linked cavity configuration of the basal water conduit system. *Journal of Geophysical Research: Solid Earth*, 92(B9), 9083–9100.

Khan, S. A., Kjeldsen, K. K., Kjær, K. H., Bevan, S., Luckman, A., Aschwanden, A., Bjørk, A. A., Korsgaard, N. J., Box, J. E., van den Broeke, M., van Dam, T. M., & Fitzner, A. (2014). Glacier dynamics at Helheim and Kangerdlugssuaq glaciers, southeast Greenland, since the Little Ice Age. *The Cryosphere*, 8(4), 1497–1507.

Kopp, R. E., Horton, R. M., Little, C. M., Mitrovica, J. X., Oppenheimer, M., Rasmussen, D. J., Strauss, B. H., & Tebaldi, C. (2014). Probabilistic 21st and 22nd century sea-level projections at a global network of tide-gauge sites. *Earth's Future*, 2(8), 383–406. 2014EF000239.

Krabill, W., Hanna, E., Huybrechts, P., Abdalati, W., Cappelen, J., Csatho, B., Frederick, E., Manizade, S., Martin, C., Sonntag, J., Swift, R., Thomas, R., & Yungel, J. (2004). Greenland Ice Sheet: Increased coastal thinning. *Geophysical Research Letters*, 31(24).

Lea, J. M., Mair, D. W. F., Nick, F. M., Rea, B. R., Weidick, A., Kjær, K. H., Morlighem, M., Van As, D., & Schofield, J. E. (2014). Terminus-driven retreat of a major southwest Greenland tidewater glacier during the early 19th century: insights from glacier reconstructions and numerical modelling. *Journal of Glaciology*, 60(220), 333–344.

Lenaerts, J. T., Van Den Broeke, M. R., Scarchilli, C., & Agosta, C. (2012). Impact of model resolution on simulated wind, drifting snow and surface mass balance in Terre Adelie, East Antarctica. *Journal of Glaciology*, 58(211), 821–829.

Lenaerts, J. T. M., Lhermitte, S., Drews, R., Ligtenberg, S. R. M., Berger, S., Helm, V., Smeets, C. J. P. P., Broeke, M. R. v. d., van de Berg, W. J., van Meijgaard, E., Eijkelboom, M., Eisen, O., & Pattyn, F. (2017). Meltwater produced by wind-albedo interaction stored in an East Antarctic ice shelf. *Nature Clim. Change*, 7(1), 58–62.

Leuschen, C. & Allen, C. (2011). IceBridge MCoRDS L2 Gridded Ice Thickness, Surface, and Bottom, Helheim, NASA DAAC at the National Snow and Ice Data Center. *(doi:http://dx.doi.org/10.5067/GDQ0CUCVTE2Q.)*.

Levermann, A., Clark, P. U., Marzeion, B., Milne, G. A., Pollard, D., Radic, V., & Robinson, A. (2013). The multimillennial sea-level commitment of global warming. *Proceedings of the National Academy of Sciences*, 110(34), 13745–13750.

Ligtenberg, S., Lenaerts, J., Van Den Broeke, M., & Scambos, T. (2014). On the formation of blue ice on Byrd Glacier, Antarctica. *Journal of Glaciology*, 60(219), 41–50.

Luckman, A., Murray, T., de Lange, R., & Hanna, E. (2006). Rapid and synchronous ice-dynamic changes in East Greenland. *Geophysical Research Letters*, 33(3).

Machguth, H., Thomsen, H. H., Weidick, A., Ahlstrøm, A. P., Abermann, J., Andersen, M. L., Andersen, A. B., Bjørk, A. A., Box, J. E., Braithwaite, R. J., Bøggild, C. E., Citterio, M., Clement, P., Colgan, W., Fausto, R. S., Gleie, K., Gubler, S., Hasholt, B., Hynek, B., Knudsen, N. T., Larsen, S. H., Mernild, S. H., Oerlemans, J., Oerter, H., Olesen, O. B., Smeets, C. J. P. P., Steffen, K., Stober, M., Sugiyama, S., van As, D., van den Broeke, M. R., & van de Wal, R. S. W. (2016). Greenland surface mass-balance observations from the ice-sheet ablation area and local glaciers. *Journal of Glaciology*, (pp. 1–27).

Mackintosh, A., Golledge, N., Domack, E., Dunbar, R., Leventer, A., White, D., Pollard, D., DeConto, R., Fink, D., Zwartz, D., Gore, D., & Lavoie, C. (2011). Retreat of the East Antarctic ice sheet during the last glacial termination. *Nature*, 4(3), 195–202.

Mackintosh, A. N., Verleyen, E., O'Brien, P. E., White, D. A., Jones, R. S., McKay, R., Dunbar, R., Gore, D. B., Fink, D., Post, A. L., Miura, H., Leventer, A., Goodwin, I., Hodgson, D. A., Lilly, K., Crosta, X., Golledge, N. R., Wagner, B., Berg, S., van Ommen, T., Zwartz, D., Roberts, S. J., Vyverman, W., & Masse, G. (2014). Retreat history of the East Antarctic Ice Sheet since the Last Glacial Maximum. *Quaternary Science Reviews*, 100, 10 – 30.

McGranahan, G., Balk, D., & Anderson, B. (2007). The rising tide: assessing the risks of climate change and human settlements in low elevation coastal zones. *Environment and Urbanization*, 19(1), 17–37.

McKay, R., Golledge, N., Maas, S., Naish, T., Levy, R., Dunbar, G., & Kuhn, G. (2016). Antarctic marine ice-sheet retreat in the Ross Sea during the early Holocene. *Geology*, 44(1), 7–10.

McMillan, M., Leeson, A., Shepherd, A., Briggs, K., Armitage, T. W. K., Hogg, A., Kuipers M., P., van den Broeke, M., Noël, B., van de Berg, W. J., Ligtenberg, S., Horwath, M., Groh, A., Muir, A., & Gilbert, L. (2016). A high-resolution record of Greenland mass balance. *Geophysical Research Letters*, 43(13), 7002–7010.

McNabb, R. W. & Hock, R. (2014). Alaska tidewater glacier terminus positions, 1948–2012. *Journal of Geophysical Research: Earth Surface*, 119(2), 153–167.

Meier, M. F. & Post, A. (1987). Fast tidewater glaciers. *Journal of Geophysical Research: Solid Earth*, 92(B9), 9051–9058.

Meierbachtol, T., Harper, J., & Humphrey, N. (2013). Basal Drainage System Response to Increasing Surface Melt on the Greenland Ice Sheet. *Science*, 341(6147), 777–779.

Moon, T. & Joughin, I. (2008). Changes in ice front position on Greenland's outlet glaciers from 1992 to 2007. *Journal of Geophysical Research: Earth Surface*, 113(F2).

Moon, T. & Joughin, I. (2015). MEaSURES Annual Greenland Outlet Glacier Terminus Positions from SAR Mosaics, Version 1. *NASA National Snow and Ice Data Center Distributed Active Archive Center, Boulder, Colorado USA, doi:10.5067/DC0MLBOCL3EL, Accessed September 29, 2015*.

Moon, T., Joughin, I., Smith, B., & Howat, I. (2012). 21st-Century Evolution of Greenland Outlet Glacier Velocities. *Science*, 336(6081), 576–578.

Moon, T., Joughin, I., Smith, B., van den Broeke, M. R., van de Berg, W. J., Noël, B., & Usher, M. (2014). Distinct patterns of seasonal Greenland glacier velocity. *Geophysical Research Letters*, 41(20), 7209–7216.

Morgan, V., Delmotte, M., van Ommen, T., Jouzel, J., Chappellaz, J., Woon, S., Masson-Delmotte, V., & Raynaud, D. (2002). Relative Timing of Deglacial Climate Events in Antarctica and Greenland. *Science*, 297(5588), 1862–1864.

Morlighem, M., Rignot, E., & K., W. J. (2016). Improving Bed Topography Mapping of Greenland Glaciers Using NASA's Oceans Melting Greenland (OMG) Data. *Oceanography*, 29.

Morlighem, M., Rignot, E., Mouginot, J., Seroussi, H., & Larour, E. (2014). Deeply incised submarine glacial valleys beneath the Greenland ice sheet. *Nature*, 7(6), 418–422.

Morton, K. W. & Mayers, D. F. (2005). *Numerical Solution of Partial Differential Equations: An Introduction*. Cambridge University Press, 2 edition.

Motyka, R. J., Cassotto, R., Truffer, M., Kjedldsen, K. K., Van as, D., Korsgaard, N. J., Fahnestock, M., Howat, I., Langen, P. L., Mortensen, J., & others. (2017). Asynchronous behavior of outlet glaciers feeding Godthåbsfjord (Nuup Kangerlua) and the triggering of Narsap Sermia's retreat in SW Greenland. *Journal of Glaciology*, 63(238), 288–308.

Murray, T., Scharrer, K., James, T. D., Dye, S. R., Hanna, E., Booth, A. D., Selmes, N., Luckman, A., Hughes, A. L. C., Cook, S., & Huybrechts, P. (2010). Ocean regulation hypothesis for glacier dynamics in southeast Greenland and implications for ice sheet mass changes. *Journal of Geophysical Research: Earth Surface*, 115(F3).

Nettles, M., Larsen, T. B., Elósegui, P., Hamilton, G. S., Stearns, L. A., Ahlstrøm, A. P., Davis, J. L., Andersen, M. L., de Juan, J., Khan, S. A., Stenseng, L., Ekström, G., & Forsberg, R. (2008). Step-wise changes in glacier flow speed coincide with calving and glacial earthquakes at Helheim Glacier, Greenland. *Geophysical Research Letters*, 35(24).

Nick, F. & Oerlemans, J. (2006). Dynamics of tidewater glaciers: comparison of three models. *Journal of Glaciology*, 52(177), 183–190.

Nick, F., van der Veen, C., Vieli, A., & Benn, D. (2010). A physically based calving model applied to marine outlet glaciers and implications for the glacier dynamics. *Journal of Glaciology*, 56(199), 781–794.

Nick, F. M., van der Veen, C. J., & Oerlemans, J. (2007). Controls on advance of tidewater glaciers: Results from numerical modeling applied to Columbia Glacier. *Journal of Geophysical Research: Earth Surface*, 112(F3).

Nick, F. M., Vieli, A., Andersen, M. L., Joughin, I., Payne, A., Edwards, T. L., Pattyn, F., & van de Wal, R. S. W. (2013). Future sea-level rise from Greenland/'s main outlet glaciers in a warming climate. *Nature*, 497(7448), 235–238.

Nick, F. M., Vieli, A., Howat, I. M., & Joughin, I. (2009). Large-scale changes in Greenland outlet glacier dynamics triggered at the terminus. *Nature*, 2(2), 110–114.

Noël, B., van de Berg, W. J., van Meijgaard, E., Kuipers Munneke, P., van de Wal, R. S. W., & van den Broeke, M. R. (2015). Evaluation of the updated regional climate model RACMO2.3: summer snowfall impact on the Greenland Ice Sheet. *The Cryosphere*, 9(5), 1831–1844.

O'Neel, S., Pfeffer, W. T., Krimmel, R., & Meier, M. (2005). Evolving force balance at Columbia Glacier, Alaska, during its rapid retreat. *Journal of Geophysical Research: Earth Surface*, 110(F3).

Parrenin, F., Barnola, J.-M., Beer, J., Blunier, T., Castellano, E., Chappellaz, J., Dreyfus, G., Fischer, H., Fujita, S., Jouzel, J., Kawamura, K., Lemieux-Dudon, B., Loulergue, L., Masson-Delmotte, V., Narcisi, B., Petit, J.-R., Raisbeck, G., Raynaud, D., Ruth, U., Schwander, J., Severi, M., Spahni, R., Steffensen, J. P., Svensson, A., Udisti, R., Waelbroeck, C., & Wolff, E. (2007). The EDC3 chronology for the EPICA Dome C ice core. *Climate of the Past*, 3(3), 485–497.

Peltier, W. & Fairbanks, R. (2006). Global glacial ice volume and Last Glacial Maximum duration

from an extended Barbados sea level record. *Quaternary Science Reviews*, 25(23–24), 3322 – 3337.

Petit, J. R., Jouzel, J., Raynaud, D., Barkov, N. I., Barnola, J.-M., Basile, I., Bender, M., Chappellaz, J., Davis, M., Delaygue, G., Delmotte, M., Kotlyakov, V. M., Legrand, M., Lipenkov, V. Y., Lorius, C., PEpin, L., Ritz, C., Saltzman, E., & Stievenard, M. (1999). Climate and atmospheric history of the past 420,000 years from the Vostok ice core, Antarctica. *Nature*, 399(6735), 429–436.

Pfeffer, W. T. (2007). A simple mechanism for irreversible tidewater glacier retreat. *Journal of Geophysical Research: Earth Surface*, 112(F3).

Pollard, D. & DeConto, R. M. (2009). Modelling West Antarctic ice sheet growth and collapse through the past five million years. *Nature*, 458(7236), 329–332.

Pollard, D. & DeConto, R. M. (2012). A simple inverse method for the distribution of basal sliding coefficients under ice sheets, applied to Antarctica. *The Cryosphere*, 6(5), 953–971.

Post, A., O'Neel, S., Motyka, R. J., & Streveler, G. (2011). A complex relationship between calving glaciers and climate. *Eos, Transactions American Geophysical Union*, 92(37), 305–306.

Pralong, M. R. & Gudmundsson, G. H. (2011). Bayesian estimation of basal conditions on Rutford Ice Stream, West Antarctica, from surface data. *Journal of Glaciology*, 57(202), 315–324.

Pritchard, H. D., A., R. J., Vaughan, D. G., & Edwards, L. A. (2009). Extensive dynamic thinning on the margins of the Greenland and Antarctic ice sheets. *Nature*, 461(7266), 971–975.

Pritchard, H. D., Ligtenberg, S. R. M., Fricker, H. A., Vaughan, D. G., van den Broeke, M. R., & Padman, L. (2012). Antarctic ice-sheet loss driven by basal melting of ice shelves. *Nature*, 484(7395), 502–505.

Rignot, E., Box, J. E., Burgess, E., & Hanna, E. (2008). Mass balance of the Greenland ice sheet from 1958 to 2007. *Geophysical Research Letters*, 35(20).

Rignot, E., Fenty, I., Xu, Y., Cai, C., & Kemp, C. (2015). Undercutting of marine-terminating glaciers in West Greenland. *Geophysical Research Letters*, 42(14), 5909–5917.

Rignot, E. & Jacobs, S. S. (2002). Rapid Bottom Melting Widespread near Antarctic Ice Sheet Grounding Lines. *Science*, 296(5575), 2020–2023.

Rignot, E. & Kanagaratnam, P. (2006). Changes in the Velocity Structure of the Greenland Ice Sheet. *Science*, 311(5763), 986–990.

Rignot, E., Koppes, M., & Velicogna, I. (2010). Rapid submarine melting of the calving faces of West Greenland glaciers. *Nature Geosci*, 3(3), 187–191.

Rignot, E. & Mouginot, J. (2012). Ice flow in Greenland for the International Polar Year 2008–2009. *Geophysical Research Letters*, 39(11), n/a–n/a. L11501.

Rignot, E., Mouginot, J., & Scheuchl, B. (2011a). Antarctic grounding line mapping from differential satellite radar interferometry.

Rignot, E., Velicogna, I., van den Broeke, M. R., Monaghan, A., & Lenaerts, J. T. M. (2011b). Acceleration of the contribution of the Greenland and Antarctic ice sheets to sea level rise. *Geophysical Research Letters*, 38(5).

Sasgen, I., van den Broeke, M. R., Bamber, J. L., Rignot, E., Sørensen, L. S., Wouters, B., Martinec, Z., Velicogna, I., & Simonsen, S. B. (2012). Mass balance and acceleration of the Greenland ice sheet. (https://doi.pangaea.de/10.1594/PANGAEA.834956).

Schoof, C. (2007). Marine ice-sheet dynamics. Part 1. The case of rapid sliding. *Journal of Fluid Mechanics*, 573, 27–55.

Schoof, C. (2010). Ice-sheet acceleration driven by melt supply variability. *Nature*, 468(7325), 803–806.

Schroeder, D. V. (1999). An Introduction to Thermal Physics. *American Journal of Physics*, 67(12), 1284–1285.

Sciascia, R., Straneo, F., Cenedese, C., & Heimbach, P. (2013). Seasonal variability of submarine melt rate and circulation in an East Greenland fjord. *Journal of Geophysical Research: Oceans*, 118(5), 2492–2506.

Shepherd, A., Ivins, E. R., A, G., Barletta, V. R., Bentley, M. J., Bettadpur, S., Briggs, K. H., Bromwich, D. H., Forsberg, R.and Galin, N., Horwath, M., Jacobs, S., Joughin, I., King, M. A., Lenaerts, J. T. M., Li, J., Ligtenberg, S. R. M., Luckman, A., Luthcke, S. B., McMillan, M., Meister, R., Milne, G., Mouginot, J., Muir, A., Nicolas, J. P., Paden, J., Payne, A. J., Pritchard, H., Rignot, E., Rott, H., Sørensen, L. S., Scambos, T. A., Scheuchl, B., Schrama, E. J. O., Smith, B., Sundal, A. V., van Angelen, J. H., van de Berg, W. J., van den Broeke, M. R., Vaughan, D. G., Velicogna, I., Wahr, J., Whitehouse, P. L., Wingham, D. J., Yi, D., Young, D., & Zwally, H. J. (2012). A Reconciled Estimate of Ice-Sheet Mass Balance. *Science*, 338(6111), 1183–1189.

Shumskiy, P. & Krass, M. (1976). Mathematical Models of Ice Shelves. *Journal of Glaciology*, (pp. 419–432).

Slater, D., Nienow, P., Sole, A., Cowton, T., Mottram, R., Langen, P., & Mair, D. (2017). Spatially distributed runoff at the grounding line of a large Greenlandic tidewater glacier inferred from plume modelling. *Journal of Glaciology*.

Stearns, L. A. (2007). *Outlet glacier dynamics in East Greenland and East Antarctica*. PhD thesis, The University of Maine.

Stearns, L. A. & Hamilton, G. S. (2007). Rapid volume loss from two East Greenland outlet glaciers quantified using repeat stereo satellite imagery. *Geophysical Research Letters*, 34(5).

Stearns, L. A., Smith, B. E., & Hamilton, G. S. (2008). Increased flow speed on a large East Antarctic outlet glacier caused by subglacial floods. *Nature Geosci*, 1(12), 827–831.

Straneo, F., Curry, R. G., Sutherland, D. A., Hamilton, G. S., Cenedese, C., Vage, K., & Stearns, L. A. (2011). Impact of fjord dynamics and glacial runoff on the circulation near Helheim Glacier. *Nature Geosci*, 4(5), 322–327.

Sugiyama, S., Skvarca, P., Naito, N., Enomoto, H., Tsutaki, S., Tone, K., Marinsek, S., & Aniya, M. (2011). Ice speed of a calving glacier modulated by small fluctuations in basal water pressure. *Nature Geosci*, 4(9), 597–600.

Sutherland, D. A. & Straneo, F. (2012). Estimating ocean heat transports and submarine melt rates in Sermilik Fjord, Greenland, using lowered acoustic Doppler current profiler (LADCP) velocity profiles. *Annals of Glaciology*, 53(60), 50–58.

Sutherland, D. A., Straneo, F., & Pickart, R. S. (2014). Characteristics and dynamics of two major Greenland glacial fjords. *Journal of Geophysical Research: Oceans*, 119(6), 3767–3791.

Thomas, R. H. & Bentley, C. R. (1978). A Model for Holocene Retreat of the West Antarctic Ice Sheet. *Quaternary Research*, 10(2), 150–170.

Thomsen, H. H. & Olesen, O. B. (1991). Hydraulics and hydrology on the Inland Ice. *Grønl. Geol. Unders. Rapp*, 152, 36–38.

Timm, O. & Timmermann, A. (2007). Simulation of the Last 21 000 Years Using Accelerated Transient Boundary Conditions. *Journal of Climate*, 20(17), 4377–4401.

Truffer, M. & Motyka, R. J. (2016). Where glaciers meet water: Subaqueous melt and its relevance to glaciers in various settings. *Reviews of Geophysics*, 54(1), 220–239.

van den Broeke, M., Bamber, J., Ettema, J., Rignot, E., Schrama, E., van de Berg, W. J., van Meijgaard, E., Velicogna, I., & Wouters, B. (2009). Partitioning Recent Greenland Mass Loss. *Science*, 326(5955), 984–986.

van den Broeke, M. R. & Bintanja, R. (1995). Summertime atmospheric circulation in the vicinity

of a blue ice area in Queen Maud Land, Antarctica. *Boundary-Layer Meteorology*, 72(4), 411–438.

van den Broeke, M. R., Enderlin, E. M., Howat, I. M., Kuipers Munneke, P., Noël, B. P. Y., van de Berg, W. J., van Meijgaard, E., & Wouters, B. (2016). On the recent contribution of the Greenland ice sheet to sea level change. *The Cryosphere*, 10(5), 1933–1946.

van der Veen, C., Plummer, J., & Stearns, L. (2011). Controls on the recent speed-up of Jakobshavn Isbrae, West Greenland. *Journal of Glaciology*, 57(204), 770–782.

van der Veen, C. J. (1996). Tidewater calving. *Journal of Glaciology*, 42, 375–385.

van der Veen, C. J. (2013). *Fundamentals of Glacier Dynamics, Second Edition*. CRC Press.

van der Veen, C. J. & Whillans, I. M. (1996). Model experiments on the evolution and stability of ice streams. *Annals of Glaciology*, 23, 129–137.

Vieli, A., Funk, M., & Blatter, H. (2000). Tidewater glaciers: frontal flow acceleration and basal sliding. *Annals of Glaciology*, 31(1), 217–221.

Vieli, A. & Nick, F. M. (2011). Understanding and Modelling Rapid Dynamic Changes of Tidewater Outlet Glaciers: Issues and Implications. *Surveys in Geophysics*, 32(4), 437–458.

Vieli, A. & Payne, A. J. (2005). Assessing the ability of numerical ice sheet models to simulate grounding line migration. *Journal of Geophysical Research: Earth Surface*, 110(F1), n/a–n/a. F01003.

Weertman, J. (1974). Stability of the Junction of an Ice Sheet and an Ice Shelf. *Journal of Glaciology*, 13(67), 3–11.

Whillans, I. M. & van Der Veen, C. J. (1997). The role of lateral drag in the dynamics of Ice Stream B, Antarctica. *Journal of Glaciology*, 43(144), 231–237.

Whitehouse, P. L., Bentley, M. J., & Brocq, A. M. L. (2012). A deglacial model for Antarctica: geological constraints and glaciological modelling as a basis for a new model of Antarctic glacial isostatic adjustment. *Quaternary Science Reviews*, 32, 1 – 24.

Whitehouse, P. L., Bentley, M. J., Vieli, A., Jamieson, S. S. R., Hein, A. S., & Sugden, D. E. (2017). Controls on Last Glacial Maximum ice extent in the Weddell Sea embayment, Antarctica. *Journal of Geophysical Research: Earth Surface*, 122(1), 371–397. 2016JF004121.

Yokoyama, Y., Anderson, J. B., Yamane, M., Simkins, L. M., Miyairi, Y., Yamazaki, T., Koizumi, M., Suga, H., Kusahara, K., Prothro, L., Hasumi, H., Southon, J. R., & Ohkouchi, N. (2016). Widespread collapse of the Ross Ice Shelf during the late Holocene. *Proceedings of the National Academy of Sciences*, 113(9), 2354–2359.